Extended Neutral Hydrogen in the Aligned Shell Galaxies Arp 230 and MCG -5-7-1

Schiminovich, David; van Gorkom, J. H.; van der Hulst, J. M.

Published in:
The Astronomical Journal

DOI:
10.1088/0004-6256/145/2/34

Publication date:
2013

The Astronomical Journal, 145:34 (20pp), 2013 February doi:10.1088/0004-6256/145/2/34

EXTENDED NEUTRAL HYDROGEN IN THE ALIGNED SHELL GALAXIES Arp 230 AND MCG −5-7-1: FORMATION OF DISKS IN MERGING GALAXIES?

David Schiminovich[1], J. H. van Gorkom[1], and J. M. van der Hulst[2]
[1] Department of Astronomy, Columbia University, New York, NY 10027, USA
[2] Kapteyn Astronomical Institute, 9700-AV Groningen, The Netherlands
Received 2011 June 19; accepted 2012 August 16; published 2013 January 9

ABSTRACT

As part of an ongoing study of the neutral hydrogen (H I) morphology and kinematics of "shell" elliptical galaxies, we present Very Large Array observations of two shell galaxies with aligned shells, Arp 230 and MCG −5-7-1. Our data provide the first H I images of Arp 230 and deeper images of MCG −5-7-1 than previously reported. Optical images of Arp 230 reveal a bright, aligned, interleaved shell system, making it an ideal candidate for "phase-wrapped" shell formation following a radial encounter with a smaller companion. The fainter, non-interleaved shells of MCG −5-7-1 do not clearly favor a particular formation scenario. The H I we detect in both galaxies extends to nearly the same projected distance as the optical shells. In Arp 230 this gas appears to be anti-correlated with the aligned shells, consistent with our expectations for phase-wrapped shells produced in a radial encounter. In MCG −5-7-1, we observe gas associated with the shells making a "spatial wrapping" or looping scenario more plausible. Although the extended gas component in both galaxies is unevenly distributed, the gas kinematics are surprisingly regular, looking almost like complete disks in rotation. We use the H I kinematics and optical data to determine mass-to-light ratios M/L_B of $2.4^{+3.0}_{-0.5}$ (at 13.5 kpc, 4.5 R_e) for Arp 230 and M/L_B of 30 ± 7 (at 40 kpc, 7 R_e) in MCG −5-7-1. In both systems we find that this ratio changes as a function of radius, indicating the presence of a dark halo. By comparing orbital and precession timescales, we conclude that the potentials are slightly flattened. We infer a 5%–10% flattening for Arp 230 and less flattening in the case of MCG −5-7-1. Finally, we present images of the H I associated with the inner disk or (polar) ring of each galaxy and discuss possible explanations for their different present-day star formation rates. We detect total H I masses of $1.1 \times 10^9 M_\odot$ in Arp 230 and $3.7 \times 10^9\ M_\odot$ in MCG −5-7-1. Both systems have H I masses, scale sizes, and regular kinematics similar to those of non-aligned shell galaxies we have previously studied (Cen A and NGC 2865). Furthermore, we (re-)emphasize in this paper that shell galaxies such as MCG −5-7-1, along with previously studied galaxies NGC 5128 (Cen A) and NGC 2865, are unique in that they provide evidence of recent accretion with gas and collisionless stars showing clear association, though the displacement suggests the presence of significant gas-dynamical interaction.

Key words: galaxies: elliptical and lenticular, cD – galaxies: interactions – galaxies: ISM – galaxies: peculiar

Online-only material: color figure

1. INTRODUCTION

Faint stellar shells—optically detected arcs, loops, and ripples—are not uncommon in field elliptical galaxies (Malin & Carter 1983; Schweizer & Seitzer 1988; and for recent work, e.g., Hernández-Toledo et al. 2008). Less frequent are the more celebrated subset of shell galaxies, those with aligned shells (e.g., NGC 3923, NGC 1344) with arcs falling along an axis, and opposing features occasionally interleaved in radius. These galaxies were the subject of early simulations of shell galaxies (Quinn 1984) which showed quite convincingly that aligned shells could be produced through the destruction of a small companion following radial infall into a larger galaxy's potential well. Stars from the secondary oscillate or "phase wrap" within the larger potential, with shells resulting from brightness enhancements due to orbit crowding at turning points.

Quinn's (1984) and subsequent simulations also showed that non-radial encounters could produce non-aligned shells. Hernquist & Quinn (1988, 1989) generalized the models further by making shells in spherical and non-spherical potentials, and from a variety of encounter scenarios—including accretion of material from a passing companion. Hernquist & Quinn also generalized the definition of "shell" to include features which are simply edge-brightened due to projection effects ("spatial wrapping"), rather than orbit crowding ("phase wrapping").[3] This generalization severely handicapped attempts to use shell morphology to study the potential of ellipticals, but simultaneously provided an explanation for the ubiquity of shell features in field ellipticals. Subsequent simulations of Hernquist & Spergel (1992) extended this argument and found that aligned and non-aligned shell features could result following a major merger, thus broadening the scope of shell-producing phenomena to include the entire spectrum of accretion and merging events.

Extended debris such as shells very likely retain some memory of the event that formed them in their kinematics (Barnes & Hernquist 1996, 1998). However, obtaining optical spectroscopy of shells is extremely difficult, due to their low surface brightness (typically $\mu_B < 24.0$). Shell morphology can be used as a signature of an accretion event in the galaxy's recent past, and the strength of the shell structure has been applied in an attempt to date the age of merger remnants (Schweizer & Seitzer 1992). In general, studies of elliptical galaxies with shells rarely consider the precise shell morphology other than as a signature of a recent accretion event (e.g., van Dokkum et al. 2004; Tal & van Dokkum 2011).

[3] See Figure 9 of Hernquist & Quinn (1988) for a good illustration of the differences between phase and spatial wrapping in several phase space projections.

Past and recent developments suggest that further attention to shell morphology could provide valuable information about the growth of galaxies, particularly in light of current ΛCDM models and the hierarchical picture of galaxy formation and evolution. Below we cite three particular examples, but also note that the development of this subject remains relatively immature, in part due to the observational challenges described above and the theoretical challenges of modeling dark matter, gas, and stars in the outer parts of galaxies with high fidelity.

The discovery of H I associated with the shells of Cen A and NGC 2865 (Schiminovich et al. 1994, 1995) showed that in some systems the picture must be far more complex than early models have suggested. In both of these galaxies gas was observed associated with shells at extended radii, slightly displaced to the outside of the stellar shells. The H I is smoothly and rapidly rotating with the same sense of rotation as the underlying galaxy. Radial encounters are expected to produce violent gas infall; gas is not expected to survive the orbit crossings of the phase-wrapping process. While such dissipation may be different for molecular gas that is more strongly clumped (Combes & Charmandaris 1999; Charmandaris et al. 2000) the H I in both galaxies very likely supports a scenario of "spatially wrapped" formation of the shells in these systems, possibly following a major merger. This is consistent the "all-around" morphology of the shells in these galaxies. Nevertheless, the gas–shell association remains puzzling as the amount of extended gas, and the displacement to the outside, is in disagreement with the results of shell-producing simulations which predict that in a variety of encounter geometries most of the gas rapidly segregates from the stars and sinks to the center of the main body (Weil & Hernquist 1993; Hernquist & Weil 1992; Mihos & Hernquist 1994, 1996). Barnes (2002) and very recent work, discussed below, may suggest a connection between the gas fraction of the progenitors and the structure and gas distribution in the remnant, but the extended gas–star morphology has not yet been modeled in detail.

More recent observations have revealed extensive substructure (streams) in the halo of the Milky Way and M31, with hints of similar substructure in deep imaging of nearby disk galaxies (e.g., NGC 5907; Martínez-Delgado et al. 2008). Gaseous streamers have also been discovered, a fraction of which may have an associated stellar component. In the case of the Local Group, this substructure very likely traces material stripped from lower luminosity galaxies than those that comprise shells in ellipticals. However, the message from these studies—that substructure is ubiquitous around spirals—would appear to establish a connection between spirals and ellipticals in a unified model of galaxy growth.

A subset of shell galaxies appear to show ring-like features, and in a number of cases they also have prominent polar rings. Past models have suggested that polar rings are formed either in an episode following a major merger, as part of a gaseous stripping event or due to dynamical evolution of disks and rings in a triaxial potential (Brook et al. 2008). In fact, more recent work suggests that some polar rings may arise from angular momentum alignment during continuous accretion of gas during hierarchical structure formation, and in many cases this continuous accretion can feed the growth of a sizable polar disk (Brook et al. 2008).

All three of the above examples would appear to link fine structure ("all-around" shells, tidal streamers, and polar rings) with growth in disks in the inner and outer parts of galaxies. Would we expect early-type galaxies with aligned shells to be a distinct class of object? Recent modeling suggests that in ΛCDM, infalling satellites may be on predominantly radial orbits and the effect on the disk may be nonlinear in the mass ratio (Hopkins et al. 2009), with negligible effects for 1:10 ratios. Hopkins et al. (2009) also show that the progenitor gas fractions are particularly important for determining whether the resulting merger will host a prominent thin disk component. If radial infall may also avoid the pitfalls of disk heating, and possibly provide new fuel for a central disk, then we might ask whether these encounters too might also contribute substantially to disk galaxy growth?

With these questions in mind, we present sensitive new observations of the neutral hydrogen in the two aligned shell galaxies Arp 230 (IC 51) and MCG −5-7-1 (ESO 415-G 026), two galaxies where "phase-wrapping" formation of aligned shells seems plausible. This paper provides the first maps of the H I in Arp 230, as well as new high-resolution images of the polar-ring galaxy MCG −5-7-1. Both galaxies have a diffuse extended component that shows an association (and anti-association) with the outer shell structure and a gas component associated with an inner disk or (polar) ring.

Our principal aim in this paper is to present the new images and kinematics of these two systems. We discuss the relationship of the gas to the stellar shells. We speculate on the formation history, comparing and contrasting these two somewhat unusual and peculiar, yet prototypical galaxies, also considering how Arp 230 and MCG −5-7-1 compare to the rest of the galaxy population. Finally, combining our results with previous measurements of these two systems, we explore the connection between the formation of these aligned shell systems, cosmological infall, and disk galaxy destruction and growth. As part of this study we also explore the recent star formation history of these systems. We also briefly consider the possible effects of local environment.

Throughout this paper, we take $H_0 = 70$ Mpc^{-1} km^{-1} s. The optical *B*- and *V*-band data used in Figure 1 and in the overlays were obtained at the CTIO 1 m in 1995 January.

2. PREVIOUS WORK

2.1. Arp 230

First detected as a "peculiar" galaxy by Arp (1966) who noted the "faint arcs," Arp 230 (Figure 1) is considered to be a prototype for the classic Quinn (1984) model of shell formation, where shells are formed by phase wrapping following radial accretion of cold stellar material. Arp 230 has an aligned and interleaved system of at least eight bright, sharp shells, with a shell axis nearly coincident with the major axis of the galaxy (Prieur 1988). Arp 230, like the even more prolific NGC 3923, is rather exceptional among shell galaxies, most of which have fewer and less distinct shells. That the shells in Arp 230 resulted from an accretion or merger event is supported by the fact that the most distant "shell" (at 93″) is connected to the main stellar body by a faint distorted tail or plume.

As shown in the schematic diagram in Figure 2(a), Arp 230 is unusual for other reasons: Arp 230 is a small galaxy, with a stellar luminosity $L_B = 9.7 \times 10^9\ L_\odot$ and a D_{25} of only 10 kpc (see also Table 1). Interestingly, deep images of the galaxy and its associated shell system are reminiscent of bars seen in barred spiral galaxies. The galaxy has a warped dust lane perpendicular to its major axis—a polar ring or disk. Filamentary features

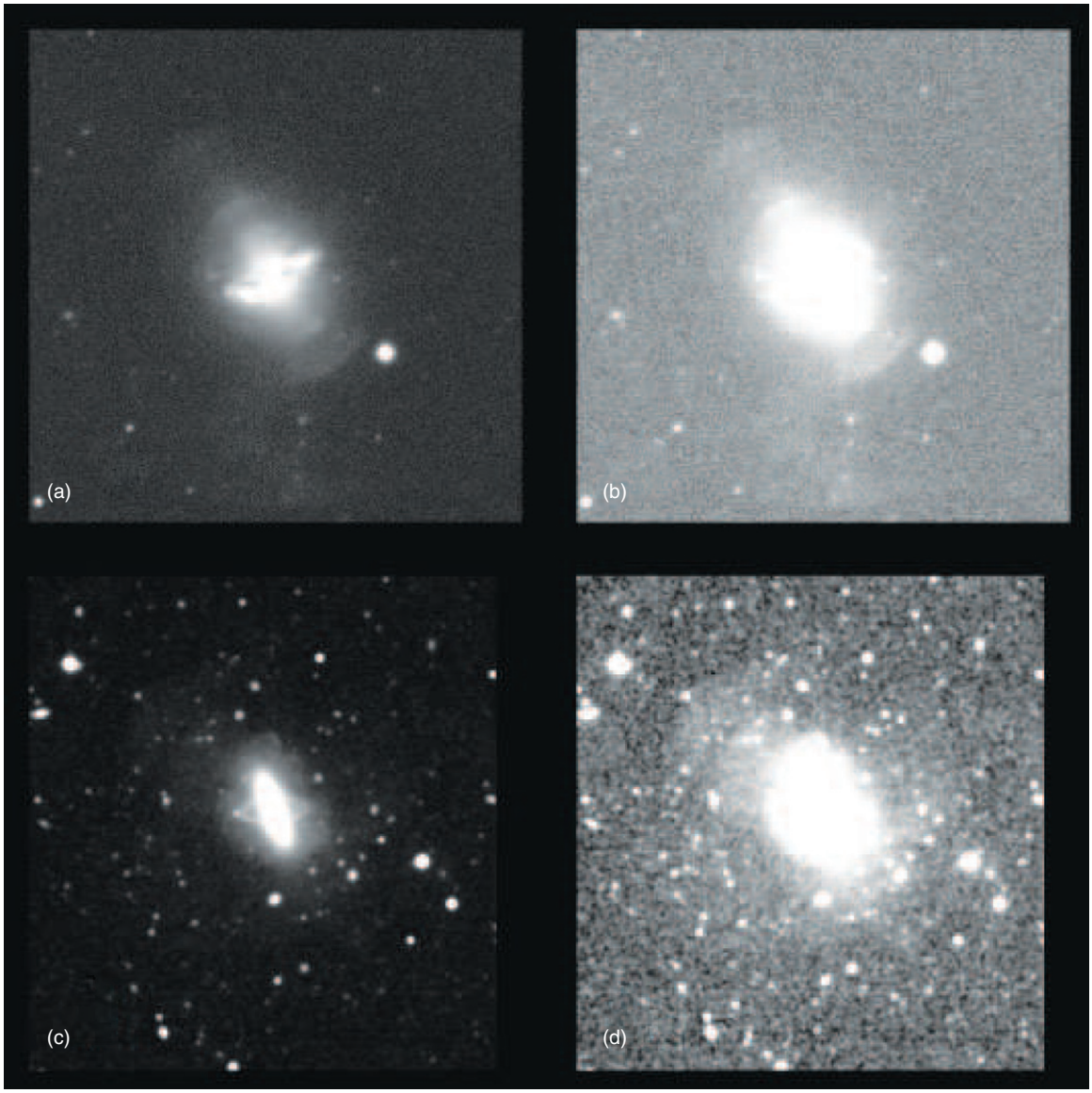

Figure 1. *B*-band image of Arp 230 (a and b) and *V*-band image of MCG −5-7-1 (c and d) taken at the CTIO 1 m telescope with contrast set to reveal the central disk/polar ring ((a) and (c)) and the outer shell structures ((b) and (d)).

or loops appear to protrude from the dust lane on each side (McGaugh & Bothun 1990). Unusual for ellipticals and shell galaxies alike, Arp 230 is an *IRAS* source (Wilkinson et al. 1987; Thronson et al. 1989), with far-infrared colors and fluxes typical of late-type spirals; star formation appears to be occurring within the dust lane. This conclusion is supported by detections of CO (Galletta et al. 1997).

McGaugh & Bothun (1990) studied the photometric properties of Arp 230. Determining shell colors is fraught with difficulties and there is little agreement on systems that have been studied by more than one group (Prieur 1990). But for Arp 230, McGaugh & Bothun (1990) find—in agreement with Prieur (1988)—that the shells are bluer than the main body of Arp 230—indicating that recent (<5 Gyr) weak bursts of star formation may have produced some of the stars seen in the stellar shells. These findings, together with the overall optical appearance and the fact that Arp 230 has no nearby companions, lead McGaugh & Bothun (1990), like Schweizer (1983), to conclude that a major merger is responsible for the creation of Arp 230.

2.2. *MCG −5-7-1*

Discovered by Arp & Madore (1986), MCG −5-7-1 is one of the six kinematically confirmed polar rings in the polar-ring catalog (Whitmore et al. 1990). It is a member of the class of narrow polar rings, with a faint slender ring (2″ thick) encircling a highly inclined S0 galaxy. Whitmore et al. (1987) conducted a in-depth optical study and van Gorkom et al. (1987) mapped this galaxy in H I. Both groups identified a disturbed extended stellar envelope and identified shells to the NE. Figure 2(b) shows a schematic diagram of MCG −5-7-1 with additional shells identified. MCG −5-7-1 has an aligned (though not interleaved) system of ∼6 faint stellar shells (see also Table 1).

Whitmore et al. (1987) find that the colors of the stellar debris are quite red, though bluer than the S0, suggesting that the accreted material is an old population, with little recent star formation. This is in sharp contrast with the bluer shells of Arp 230 and NGC 2865 (Fort et al. 1986). The ring is considerably bluer than the shells and the S0. Hα emission is detected in the ring, evidence for recent or ongoing star formation.

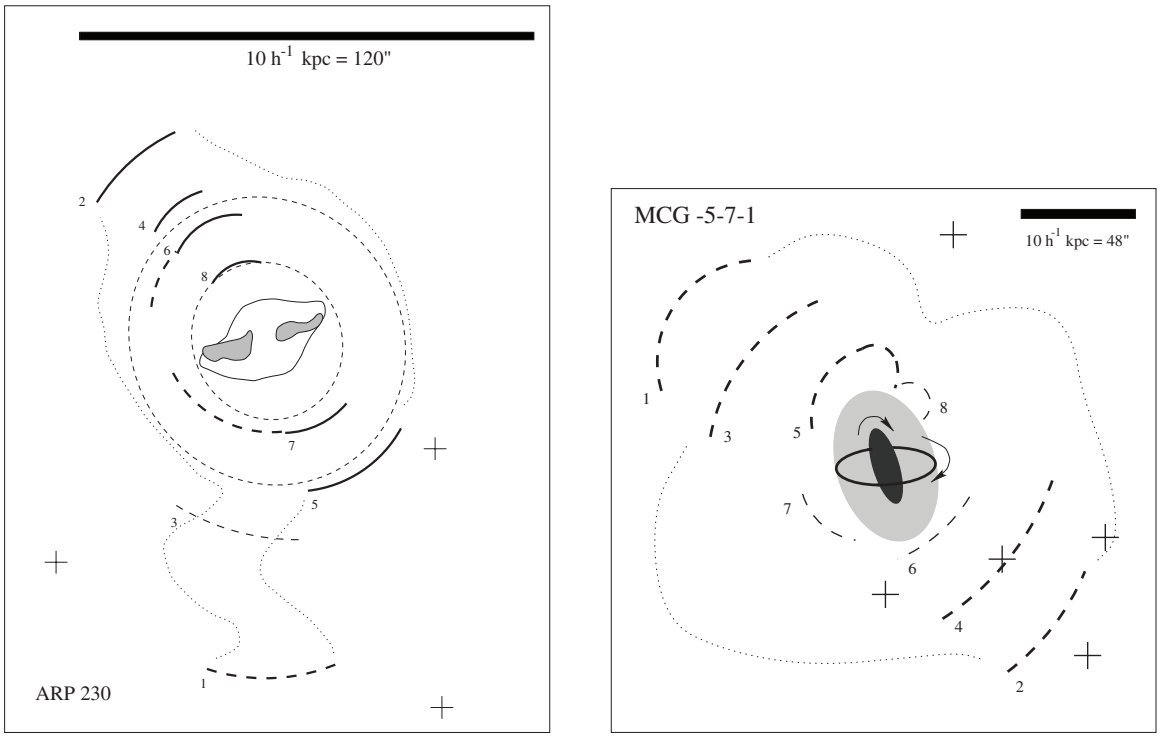

Figure 2. Schematic illustration of central disk/polar ring and outer structure of Arp 230 (a) and MCG −5-7-1 (b), respectively. Star positions in the field are indicated by + symbols. Hatched regions denote dust. Dotted lines indicate fainter structures.

Table 1
Source Data

Parameter	Arp 230	MCG −5-7-1
Right ascension (1950)	$00^h43^m53\overset{s}{.}6$	$02^h26^m11\overset{s}{.}5$
Declination (1950)	$-13°42'55''$	$-32°06'14''$
Optical velocity	1742 ± 35	4604 ± 14
Classification	S0 pec	S0 pec
B magnitude	13.41 ± 0.18	14.6 ± 0.2
Central galaxy component		
Major axis P.A.	30°	17°
Inclination	−44°	$74° \pm 4°$
Galaxy $B-V$	0.75 ± 0.05	1.02 ± 0.03
Ring component		
Polar-ring radius	n/a	$19\overset{''}{.}5$
Polar-ring P.A.	n/a	$93° \pm 1°$
Inclination	n/a	$68° \pm 2°$
Corrected rotational velocity (km s^{-1})	n/a	186 ± 2
Ring $B-V$	0.4 ± 0.05	0.90 ± 0.08
Shell component		
Shell axis P.A.	$40° \pm 5°$	$47° \pm 5°$
Number of detected shells	8	8
Shell $B-V$	n/a	0.65 ± 0.08

MCG −5-7-1 is not an *IRAS* source. The stellar component in the ring is very weak, only 1% of the luminosity of the S0. Corrected rotational velocities of the ring and the S0 are similar suggesting that MCG −5-7-1 has a spherical halo. Whitmore et al. (1987) conclude that the present form of MCG −5-7-1 probably resulted from a major merger within the last 1–3 Gyr, similar to van Gorkom et al. (1987) who concluded that MCG −5-7-1 may have resulted from the recent accretion of a gas-rich companion.

3. OBSERVATIONS

Our observations of neutral hydrogen in Arp 230 and MCG −5-7-1 were made using the Very Large Array (VLA) during the period between 1993 December and 1996 October. We measured fluxes and velocities of the neutral hydrogen component using emission from the H I hyperfine transition at 21.1 cm (1420.4 MHz). Arp 230 was observed using VLA D, C, and B configurations (with longest spacings 1.03, 3.4, and 11.4 km, respectively). MCG −5-7-1 was observed with D configuration and the hybrid C-north-B (CnB) configuration; the extended north arm of the array compensates for the N–S baseline shortening due to the low declination of MCG −5-7-1, producing a rounder, though still elongated, beam. We used instrumental resolutions of 10–40 km s^{-1} (48–195 kHz) and, wherever possible, we made use of online Hanning smoothing to reduce effects of bandpass "ringing" induced in the correlator by the Gibbs phenomenon and strong monochromatic signals. For both galaxies we used 3C48 as a flux and bandpass calibrator, with the flux determined from the Baars et al. (1977) flux scale. Phase calibrators (∼1 Jy) were chosen to be as close to the target as possible. Table 2 provides an observational summary for the new observations of Arp 230 and MCG −5-7-1.

The D configuration observation of Arp 230 was for exploratory purposes and is not used in this paper. Inside the 30′ VLA primary beam we detected H I only within the five central channels within a <3′ diameter region (∼3 beamwidths) centered on Arp 230. Subsequent observations with B- and C-array configurations were aimed toward better spatially and kinematically resolving the H I so that we could connect features observed in the H I with optical features in this peculiar galaxy.

Despite the narrow (∼200 km s^{-1}) line width for Arp 230 we maintained a wide velocity coverage in order to search for faint unresolved H I at the same velocities as CO

Table 2
Summary of Observations

Object	Observation Date	Configuration	Time (hr)[a]	ΔV (km s^{-1})	Online Hanning
ARP 230	1993 Dec 30	D	2	41.6	Y
	1994 Jul 28, 29, 30, 31	B	25	20.8	N
	1994 Aug 2	B	6.25	20.8	N
	1994 Nov 5, 6, 7	C	19	20.8	N
MCG −5-7-1	1994 Oct 4, 5, 6	CnB	12	10.5	Y
	1996 Oct 6	D	2	10.5	Y

Note. [a] Time on source is the scheduled time on source.

Table 3
Parameters for Deconvolved Image Data Cubes

Parameter	Arp 230 B	Arp 230 B+C	MCG C+D
Phase center α (1950)	$00^h43^m55\overset{s}{.}0$	$00^h43^m55\overset{s}{.}0$	$02^h26^m12\overset{s}{.}0$
Phase center δ (1950)	$-13°42'50''$	$-13°42'50''$	$-32°06'14''$
Shortest spacing (m)	210	73	73
Longest spacing (m)	11400	11400	6900
Primary beam half-power width	$30'$	$30'$	$30'$
Heliocentric central velocity (km s^{-1})	1709	1709	4628
Channel width (km s^{-1})	20.8	20.8	20.9
Number of channels	63	63	31
Velocity coverage (km s^{-1})	1100–2300	1100–2300	4350–4900
Synthesized beam major, minor axis	$7\overset{''}{.}6 \times 5\overset{''}{.}6$	$15'' \times 15''$	$32\overset{''}{.}1 \times 15\overset{''}{.}2$
Beam position angle	$0\overset{\circ}{.}0$	$0\overset{\circ}{.}0$	$2\overset{\circ}{.}16$
rms 1σ noise per beam per channel	0.07	0.16	0.2
Temperature (K) 1 mJy beam^{-1}	3.1	14.3	1.2
3σ column density per channel (cm^{-2})	2.5×10^{20}	2.4×10^{19}	2.7×10^{19}

detected by Galletta et al. (1997). Our B and C configuration data had 63, 20.8 km s^{-1} channels. Due to limitations in the VLA correlator we could maintain the same velocity coverage, while doubling the velocity resolution only by observing without online Hanning smoothing (called the "normal" mode at the VLA). Line emission in our cubes was relatively weak, and we carefully monitored the effects of the Gibbs phenomenon during continuum subtraction by comparing cubes made with and without a Hanning smoothed bandpass solution.

MCG −5-7-1 had been already observed with the VLA (van Gorkom et al. 1987). In order to obtain a deeper, higher resolution data set we observed using CnB configuration for a similar duration as the van Gorkom et al. (1987) study. Improvements in the VLA system have resulted in lower system temperatures and better correlator power than the original MCG observations. The observations presented here achieve 2.5 times better sensitivity with a comparable amount of observing time. The observational parameters for both Arp 230 and MCG −5-7-1 are summarized in Tables 2 and 3.

A difficulty with observing MCG −5-7-1 is that its redshift places its H I emission close, but slightly below 1400 MHz, a frequency at which the VLA produces strong internally generated, very monochromatic radio frequency interference (RFI). This was of particular concern for us, since single-dish observations of Richter et al. (1994) detected emission blueward of 1400 MHz contrary to the findings of van Gorkom et al. (1987). A number of observing decisions helped us to resolve that problem. We chose to observe with 63, 10 km s^{-1} channels with online Hanning smoothing, and determined a central velocity of 4268 (close to systemic) which at that time of year placed the 1400 MHz signal in the center of its channel, thus reducing its effect on neighboring channel and our velocity coverage.

We reduced the data using the standard VLA data reduction procedures outlined in the AIPS Cookbook. All data sets were edited using the AIPS task TVFLG, to remove spurious signals not properly flagged by the VLA online software. For the Arp 230 data sets, we subtracted continuum emission in the UV plane using the AIPS task UVLIN (Cornwell et al. 1992). Line-free channels to use were selected after generating a line+continuum data cube. From the continuum-subtracted UV-plane visibility data we generated two natural-weighted CLEAN-ed (Clark 1980) image cubes for Arp 230; a high-resolution cube made from the B configuration data only and second, from the B and C configuration visibility data (hereafter B+C data). Because our D configuration data were observed at lower velocity resolution, we did not include the D configuration data in our final cubes. However, as described below, it does not appear that our B+C data missed any flux due to the absence of those short spacings. The Arp 230 cube is shown in Figure 3.

For the MCG −5-7-1 data, we wanted to make sure that we were not missing any flux due to missing short spacings, so we combined our CnB data with D configuration data. Note that we did not make use of the van Gorkom et al. (1987) data set, since the new VLA data are of significantly higher quality. Line+continuum cubes were generated and cleaned from the combined (C+D) UV visibility data with the AIPS task IMAGR, using a robust weighting imaging algorithm (Briggs 1995). We chose a robustness factor (1) that gave us a reasonably small beamwidth, while losing little sensitivity (<5%) due to weighting. Maps from line-free channels (excluding the three channels centered on the 1400 MHz RFI) were selected and averaged to make a continuum image. This image was subtracted from the cube to produce a final C+D H I image cube, as shown in Figure 4. Parameters for deconvolved image data cubes for both Arp 230 and MCG −5-7-1 are listed in Table 3.

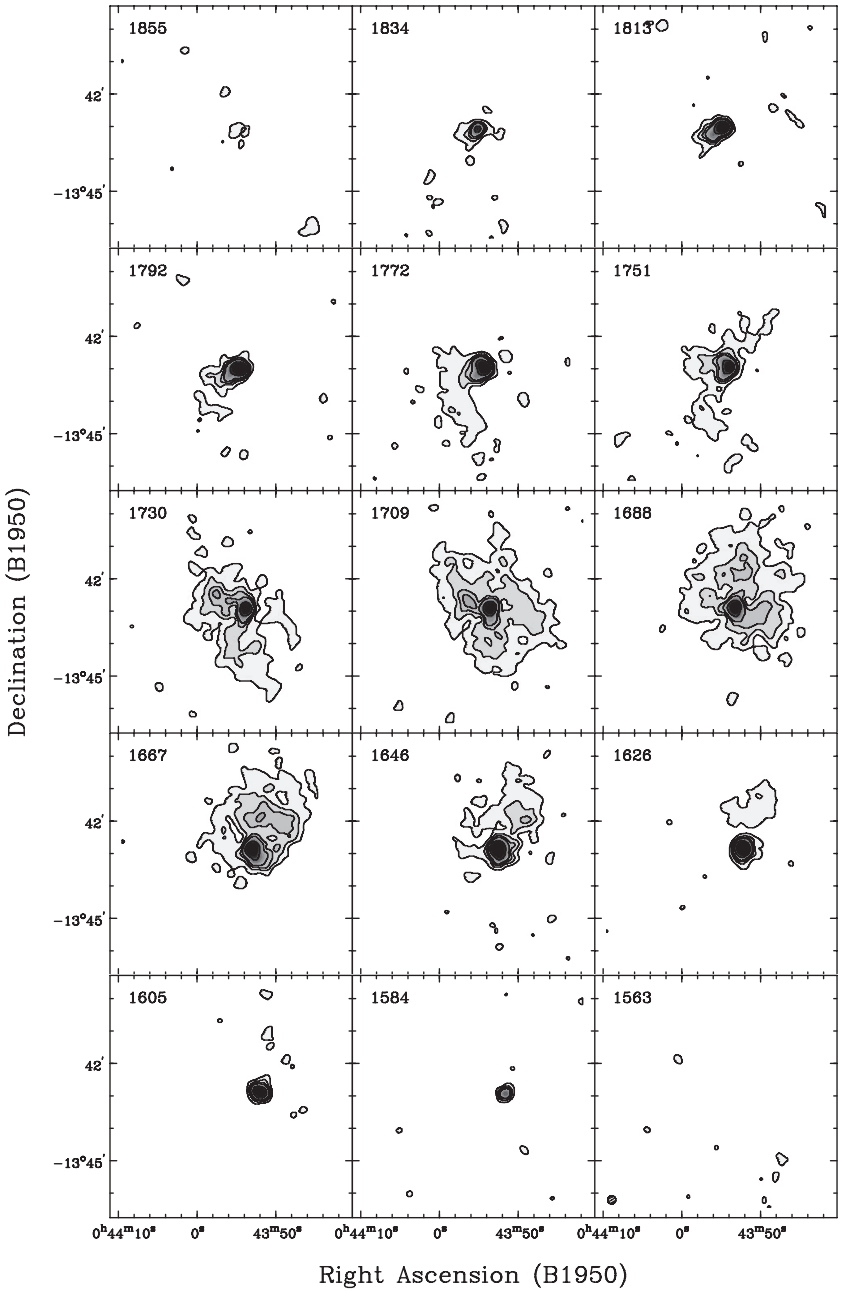

Figure 3. Channel maps of the H I emission in and around Arp 230. Contours are −0.5, 0.5, 1, 1.5, 2, 4, 8, 12, 16, and 20 mJy beam^{-1}. The heliocentric radial velocity of each channel is indicated in the top left corner. The beam is shown in the bottom right panel.

4. RESULTS

4.1. Continuum: Arp 230 and MCG −5-7-1

A continuum map of Arp 230 made from the line-free channels in the B configuration data set is shown in Figure 5. The continuum neatly traces the central dust lane. Cox & Sparke (2004) present more sensitive radio observations at 6 and 20 cm with 5″ resolution and suggest that the radio continuum emission is associated with the star formation in the disk. There is no evidence for a strong central continuum source or radio lobes extending from the nucleus. We detect no H I absorption against this weak continuum signal to a limiting optical depth of $\tau \approx 0.015$.

We did not detect continuum from MCG −5-7-1 although, like Arp 230, recent (∼1 Gyr) star formation appears to have occurred in its polar ring (Iodice et al. 2002). Nevertheless, as we discuss in Section 5.3, the specific star formation rate of MCG −5-7-1 is considerably lower than that for Arp 230 and therefore it is not surprising that the 20 cm continuum emission is fainter than our detection limit.

4.2. H I Line: Arp 230

From our data cubes we produced total H I and intensity-weighted velocity maps. Our maps were generated by smoothing the cubes in position and velocity, and only using data from the unsmoothed cube at positions in the smoothed cube that exceeded a threshold, typically between 1σ and 2σ. For all maps we tried different smoothing widths and threshold settings and chose final maps whose settings minimized contribution from sources of noise in the maps and maximized the inclusion of

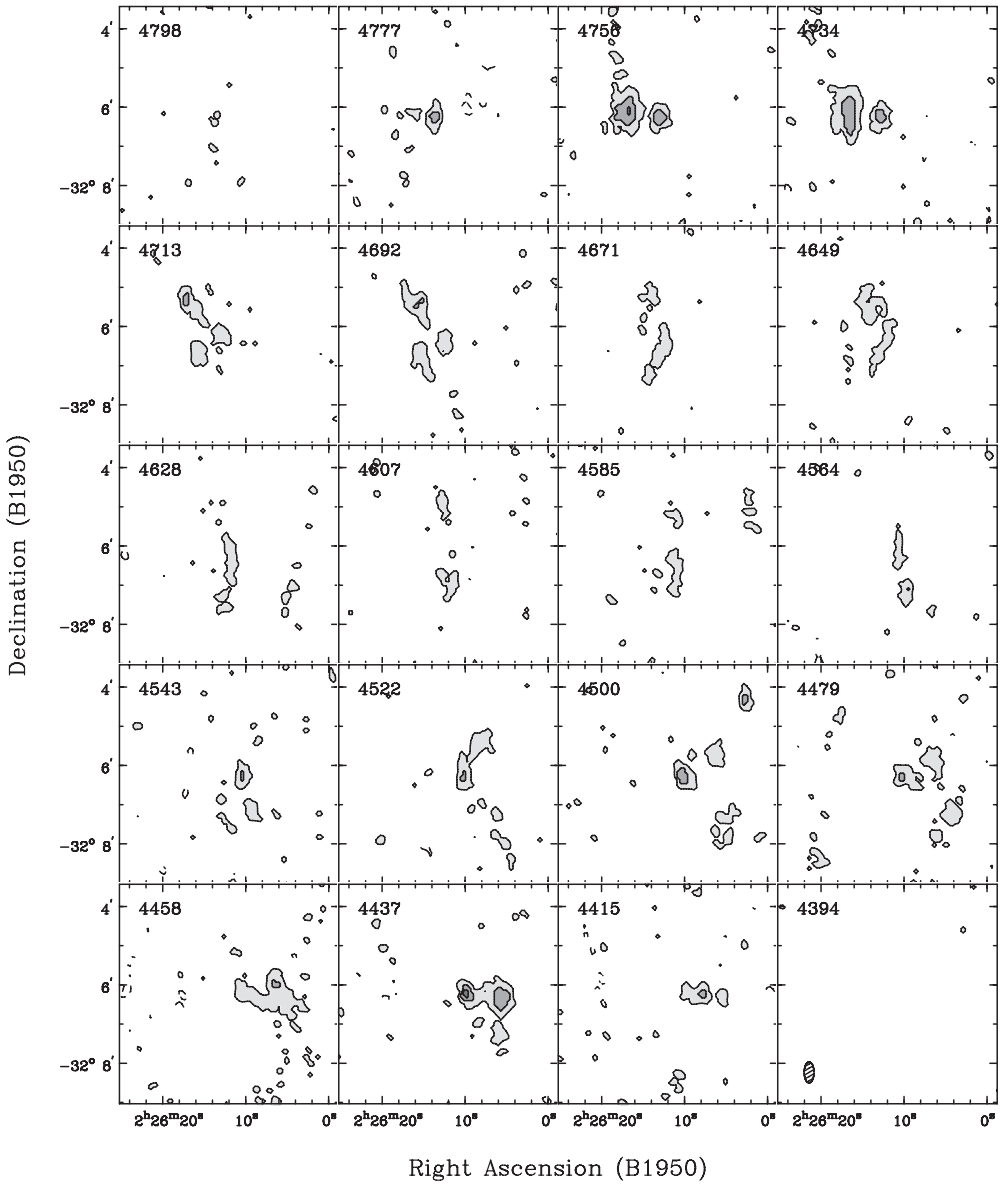

Figure 4. Channel maps of the H I emission in and around MCG −5-7-1. Contours are −0.9, 0.9, 1.8, and 2.7 mJy beam^{-1}. The heliocentric radial velocity of each channel is indicated in the top left corner. The beam is shown in the bottom right panel.

real signal from the cubes. The H I maps of Arp 230 from the B and B+C data sets are shown in Figure 6. The Moment 1 map of Arp 230 is shown in Figure 8.

The B configuration map reveals H I emission, like the continuum emission, coincident with the dust lane of Arp 230. We do not observe a gap of emission in the total H I map though an inclined and/or warped annulus could obscure a central hole. We do observe two peaks in the H I distribution appearing coincident with the regions of highest dust obscuration in the visible image. The peak column densities reach 8.4×10^{21} cm^{-2} and we set a 1.4 kpc upper limit to the inner radius of an annulus at the distance of Arp 230. The major axis of the H I in the dust lane lies at P.A. 108°, roughly perpendicular to the major axis of the central stellar body. The axis ratio of the inner H I is greater than 3:1 though it widens in the outer parts where the H I distribution becomes less regular. The P.A. of the H I matches the axis of the lane, though optically, the lane is heavily warped, especially in the inner regions (<10″).

This is the first detection of motions perpendicular to the optical major axis (P.A. 30°) of Arp 230. The velocity field, combined with the total H I map, suggests regular rotation along orbits highly inclined to our line of sight. We detect an H I central velocity of 1705 ± 3 km s^{-1} in agreement with the 1709 km s^{-1} obtained by Richter et al. (1994). Both H I velocities are ∼50 km s^{-1} lower, though not in disagreement with the optically determined systemic velocity of 1758 ± 55 km s^{-1} (Strauss et al. 1992). Although we detect strong emission in 13 channels covering a velocity range of 252 km s^{-1}, our intensity-weighted velocity map shows a range of only 170 km s^{-1}. This signature (a high velocity dispersion) is quite possibly an indication of a change in inclination or a warp in the ring. There appears to be slight kinematic evidence for an inner warp ($r < 30''$). At larger radii we do see a twist in the line of nodes, though this signature may be associated with the emission seen in the low-resolution maps.

This is well illustrated in Figure 7, a "Renzogram" (named for its inventor Renzo Sancisi) overlaid on an image of Arp 230. The

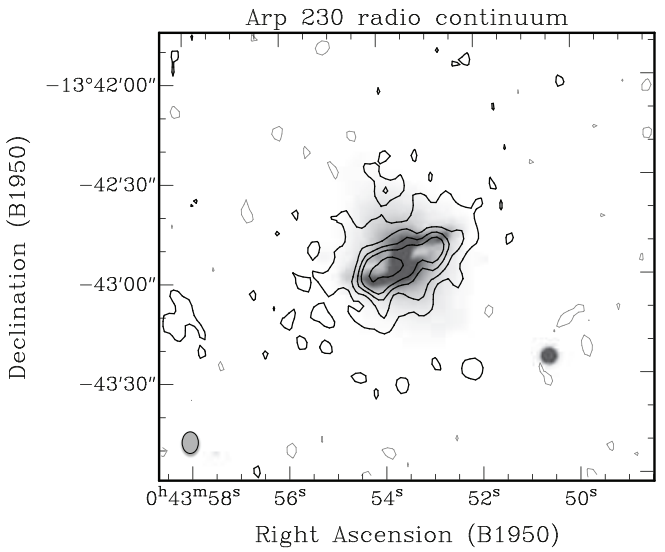

Figure 5. Radio continuum image of Arp 230 overlaid on the *B*-band image. Contours are −0.22, 0.22, 0.5, 0.75, 1, and 1.5 mJy beam^{-1}. The negative contour is shaded gray.

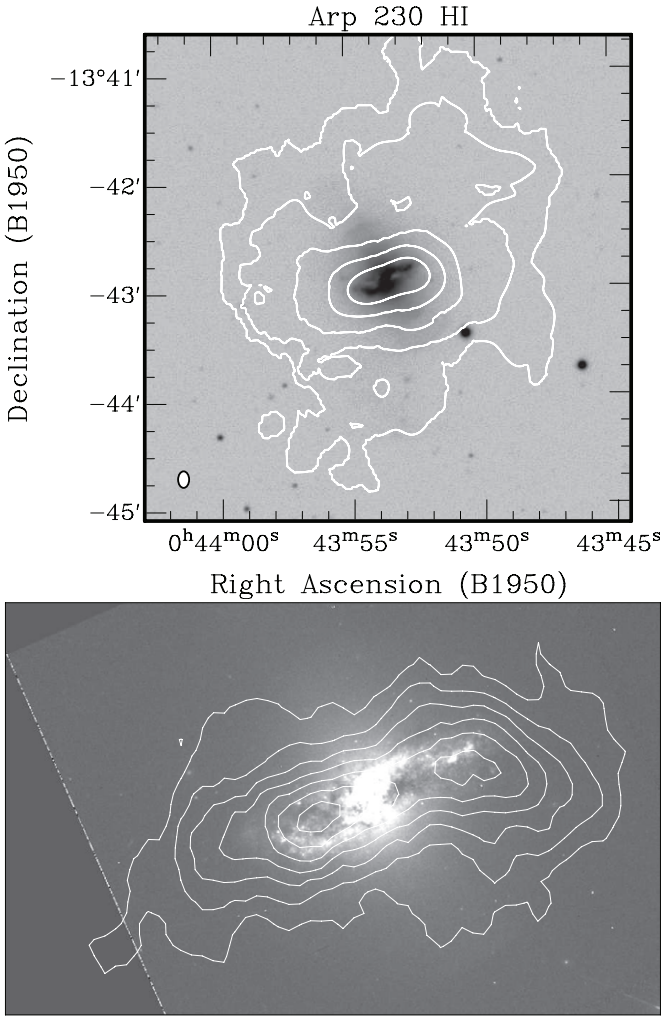

Figure 6. H I distribution overlaid on the *B*-band image of Arp 230. (B + C array data). Contours are 0.74, 1.48, 2.96, 5.92, 11.84 × 10^{20} cm^{-2}. The lower panel shows the central part of Arp 230 (90″ × 55″) with the H I distribution as determined from only the B-array data.

Renzogram, drawn by hand in the early days, puts on one plot, in different colors contours of constant brightness from each velocity channel. It is useful for detecting trends in the motions of H I between different velocity channels in ways that total H I and intensity-weighted velocity maps might obscure. Emission from all 13 channels is plotted. The contours from each channel show a positional shift with respect to the neighboring channels, though each position along the ring is contained within several contours, indicating a broad line width through the ring. The contours also indicate a bi-symmetric shift in the major axis toward P.A. 90° in the outer parts of the ring.

The B+C configuration total H I map reveals a far more extended and diffuse structure of H I than revealed by our B array maps. We detect emission at a limiting column density of 7.3 × 10^{19} cm^{-2} (15 Jy beam^{-1} m s^{-1}) extending out to 120″ (14 kpc) NW and 85″ (10 kpc) SE of the nucleus. The distribution is somewhat patchy and appears to show a minimum along the axis of the galaxy and stellar shells. The major axis of the extended H I distribution lies approximately along P.A. 150°, tilted from the major axis of the dust lane. Furthermore, the axis ratio of this extended component is less than 1.5:1, suggesting that the H I might be lying in a plane that has a low inclination to our line-of-sight distribution.

The total integrated line flux is 8.2 ± 1 Jy km s^{-1}. This line flux matches the total line flux from our D-array data (8.4 ± 1 Jy km s^{-1}), suggesting that we have not lost any signal due to short spacings. This value is 25% lower than the 11.5 ± 1.2 Jy km s^{-1} detected with single-dish by Richter et al. (1994). Since no other emission is detected in the field, we are unable to explain this discrepancy. Using a systemic velocity of 1705 km s^{-1} and an implied distance of 24.3 Mpc we obtain a total H I mass of 1.2 × 10^9 $M_\odot$.

That the extended H I component might be lying in a plane, and rotating in (nearly) circular orbits is further supported by the velocity field of the outer H I shown in Figure 8. The kinematic major axis (P.A. 135° ± 5°) is roughly aligned with the major axis of the extended H I distribution. Furthermore, the velocity field of the outer parts looks very regular, with only a twist in the kinematic line of nodes seen at the interface between the disk component and the extended component. The velocity structure of the outer H I maintains a reasonably constant P.A. and appears to be quite distinct from the central disk. Similarly, position–velocity cuts through the data cube (Figure 9) at different position angles show what appear to be two components. Once again, the plots do not look exceptionally different from what is expected for gas on circular orbits.

The regularity of the velocity fields and the reasonable agreement between the kinematics and the surface density distribution led us to attempt a tilted-ring fit (Rogstad et al. 1974; Begeman 1987, 1989) to the velocity field of Arp 230. Naturally, due to the unsettled nature of this disturbed system we must view this fit with caution, since some of the gas is very likely moving on non-circular orbits and the gas is clearly not co-planar. We therefore do not provide goodness-of-fit estimates. However, the model is useful for extracting some of the basic parameters of the system. We only allowed four parameters to vary in our fit, the systemic velocity $v_{\rm sys}$, the rotation velocity $v_{\rm rot}$, the inclination i, and the position angle θ. We do not make any correction for beam smearing. Figure 10 shows our best-fit parameters. Clearly observed is the sharp jump in the kinematic line of nodes in the outer parts. The inclination flattens out though the velocity remains reasonably constant near 80 km s^{-1}. Figure 11 shows this model as contours overlaid on

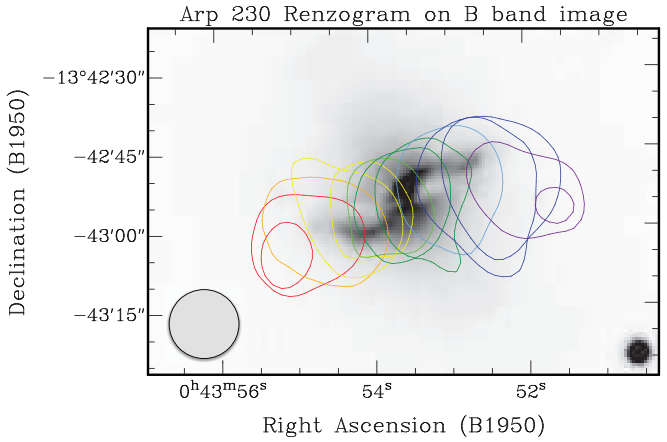

Figure 7. Renzogram of the B-array data (7.″5 × 5.″5 beam) on the optical image of Arp 230. Contour velocities are (purple) 1584, 1605, (blue) 1626, 1646, 1667, (green) 1688, 1709, (light green) 1730, (yellow) 1751, 1772, (orange) 1792, (red) 1813 and 1834 km s^{-1}. The contour value is 1.5 mJy beam^{-1} in the corresponding channels.

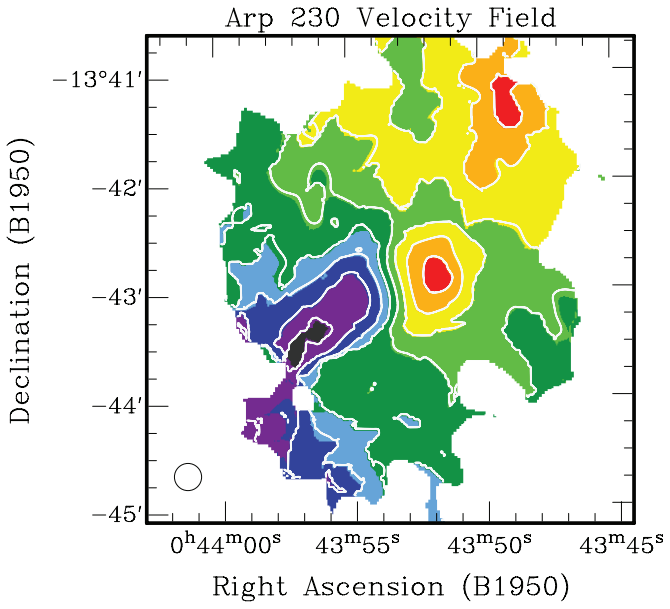

Figure 8. H I velocity field of Arp 230. Velocity contours are 1640, 1660, 1680, 1700, 1720, 1740, 1760, and 1780 km s^{-1} (from red to black).

Table 4
Derived H I Data

Parameter	Arp 230	MCG −5-7-1
Systemic velocity	1705 ± 3	4593 ± 6
Rotational velocity	85	180
Inclination (ring)	89 ± 3	54 ± 5
Inclination (outer)	31 ± 3	47 ± 5
Extent of H I	1.′8	1.′8
Period at outer radius (Myr)	771	785
$M_{\rm H\,I}$ ($M_\odot$)	1.2 × 10^9	3.7 × 10^9

the channel maps. The brightness distribution has been assumed to be azimuthally uniform. Table 4 summarizes the galaxy parameters.

4.3. H I Line: MCG −5-7-1

Using the methods described in the previous section we produced total H I line map and intensity-weighted velocity

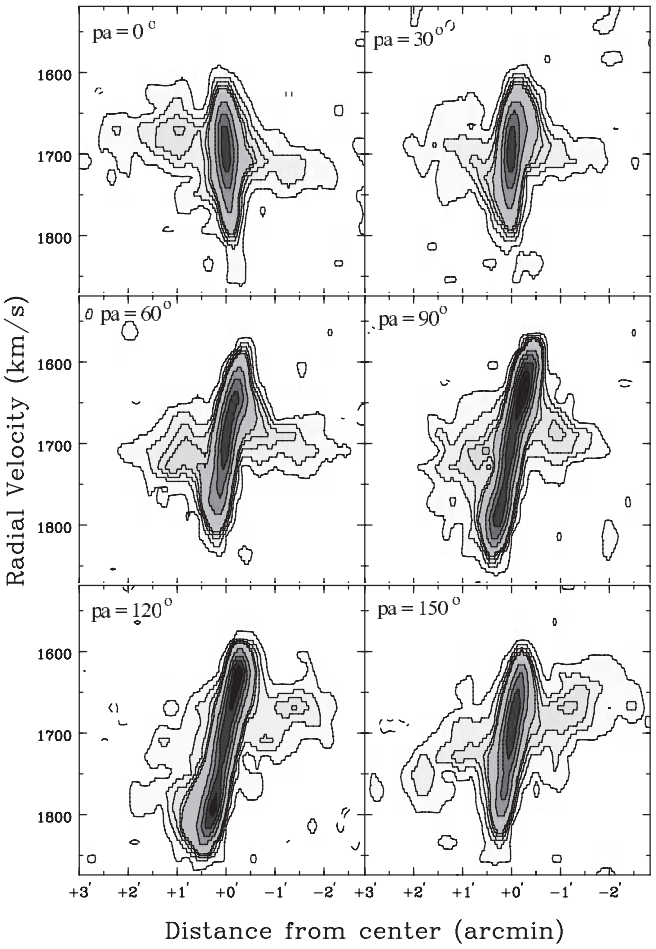

Figure 9. Position–velocity maps of the H I emission in Arp 230 at position angles of (from top left to bottom right) 0°, 30°, 60°, 90°, 120°, and 150°. Contours are −0.4, 0.4, 0.8, 1.2, 1.6, 2, 4, 6, 8, 10 mJy beam^{-1}. Major axis position angle is ∼120°.

map (Figures 12 and 13) from the C+D cube for MCG −5-7-1. Comparison with Figure 11 of van Gorkom et al. (1987) shows that the new observations reveal much more structure in the H I distribution than was previously detected, although the overall morphology of the H I (i.e., the "butterfly contours") remains much the same.

H I is detected associated with the polar ring, with a gap seen at the center of the galaxy. The P.A. of the H I matches the optical polar ring (P.A. 93° and appears to have a similar inclination. The distribution of H I in the ring is asymmetric with twice as much emission coming from the W side of the ring as the E side. Peak column densities are in excess of 10^{21} cm^{-2}, peaking at the endpoints of the ring.

Beyond the inner ring, the extended gas shows an extremely patchy morphology. In the outer regions, more gas is seen to the E than in the W. The major axis of the broken outer gas distribution, as seen in the total H I plot, lies at P.A. 60°–70°. Unlike the inclined inner ring, the extended H I appears more face-on with some hint of spiral-like structure in the contours. Arcs on the total H I plot show the locations of the optical shells. The outer gas peaks fall near—though are not clearly coincident—with the stellar shells and the H I is extended in the same direction as the axis of the shells. In the NE the curvature of the H I segment mimics that of the neighboring stellar shell, providing a weak hint that they might be related.

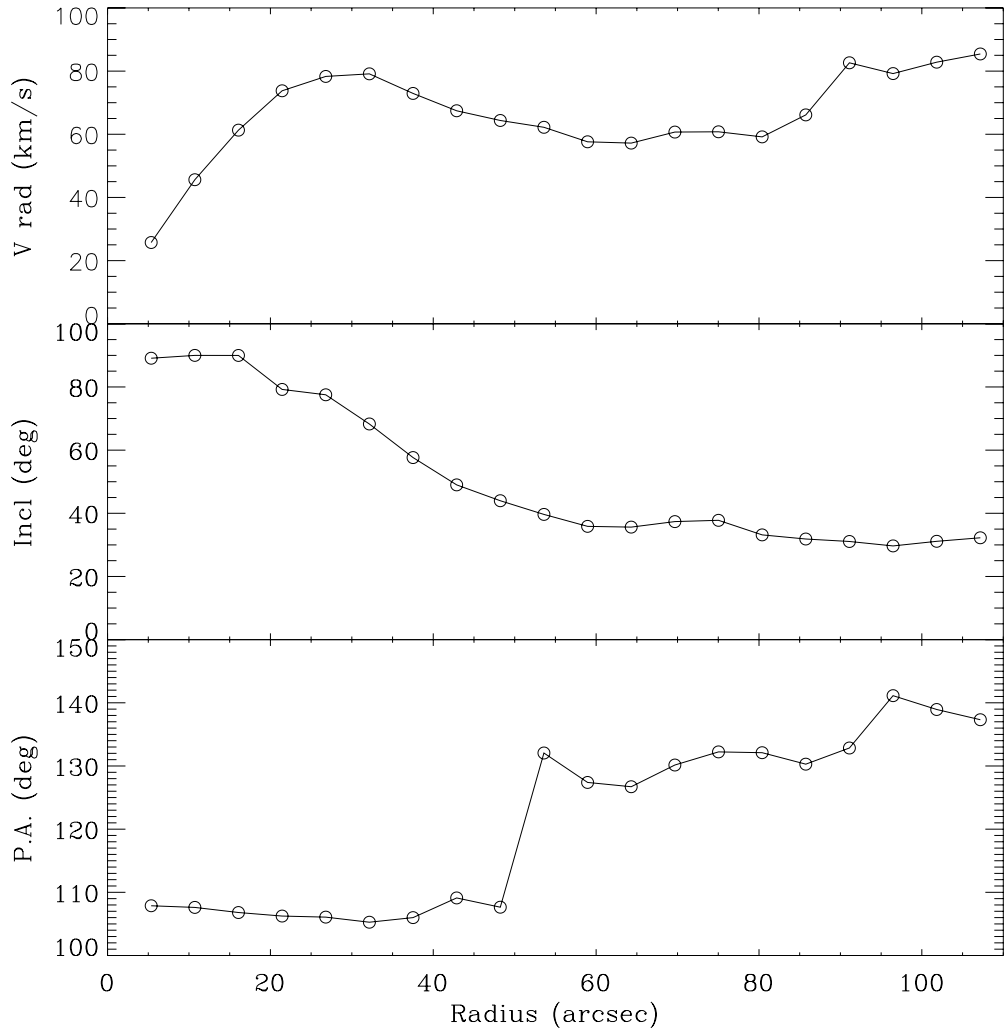

Figure 10. Rotation curve fit for Arp 230. The panels show (from top to bottom) rotation velocity, inclination, and position angle of the line of nodes as a function of radius.

We find an integrated flux of 3.4 ±.2 Jy km s^{-1}, confirming the flux measured with the VLA in van Gorkom et al. (1987). Furthermore, we find no emission in the channels blueward of the 1400 MHz VLA RFI. This total is lower than the 6.22 ± 1.8 of Richter et al. (1994) who measure a velocity width greater by some 100 km s^{-1} (mostly at velocities blueward of the VLA measurements). We do not detect emission in our cube in those channels, though emission from a galaxy 17′ to the NW with systemic velocity of 4530 km s^{-1} might be contributing to the signal in the Green Bank beam. Using a systemic velocity of 4590 km s^{-1} and an implied distance of 65.6 Mpc we obtain a total H I mass of 3.7 × 10^9 $M_\odot$.

The velocity field appears to show regular rotation, with the kinematic major axis in rough agreement with the morphological major axis. Only in the very outer parts do we observe a significant deviation, where the kinematic major axis twists only slightly, not nearly so much as the major axis of the H I distribution.

We made a rotation curve fit to the data to determine $v_{\rm sys}$, $v_{\rm rot}$, i, and θ. Model fits (Figure 14) give a $v_{\rm sys}$ of 4593 ± 6 km s^{-1} and $v_{\rm rot}$ beyond 20″ rising from 150 km s^{-1} to 200 km s^{-1}. Comparison with channel maps in Figure 15 shows a good fit, though naturally the real emission is poorly represented by a smooth surface brightness distribution. Our velocities in the inner 30″ are likely to be underestimates due to beam smearing with an average beyond that range of 182 km s^{-1}. Inclinations drop slightly from 60°–65° to 50° and P.A. gradually varies from 93° to 87°. The optical and H I parameters are shown in Tables 1 and 4. The H I has nearly the same inclination and P.A. as the polar ring (Whitmore et al. 1987), suggesting that the gas motions of the H I and Hα in the ring are similar. Inclinations at large radii are very poorly determined.

Finally, we show a position–velocity cut along P.A. 0°, 45°, 90°, and along 135° (Figure 16). The P.A. 90° plot gives the appearance of a standard disk with a flat rotation curve. The P.A. 45° plot, taken close to the shell axis reveals a nearly linear chain of discrete clouds in addition to a central high velocity component due to the ring. If we ignore the inner ring, this chain might also be interpreted as clouds along a broken circular ring.

5. DISCUSSION

In this section we principally discuss how these observations provide insight into gaseous disk formation and evolution. First, we discuss how the gasdynamics gives us insight into the structure of each galaxy and compare with other literature. Next, we describe how observations in this paper—as well as previous results—are consistent with the conclusion that the presence of shells in a galaxy implies a pre-existing cold component that may contain significant amount of gas. Finally, we address

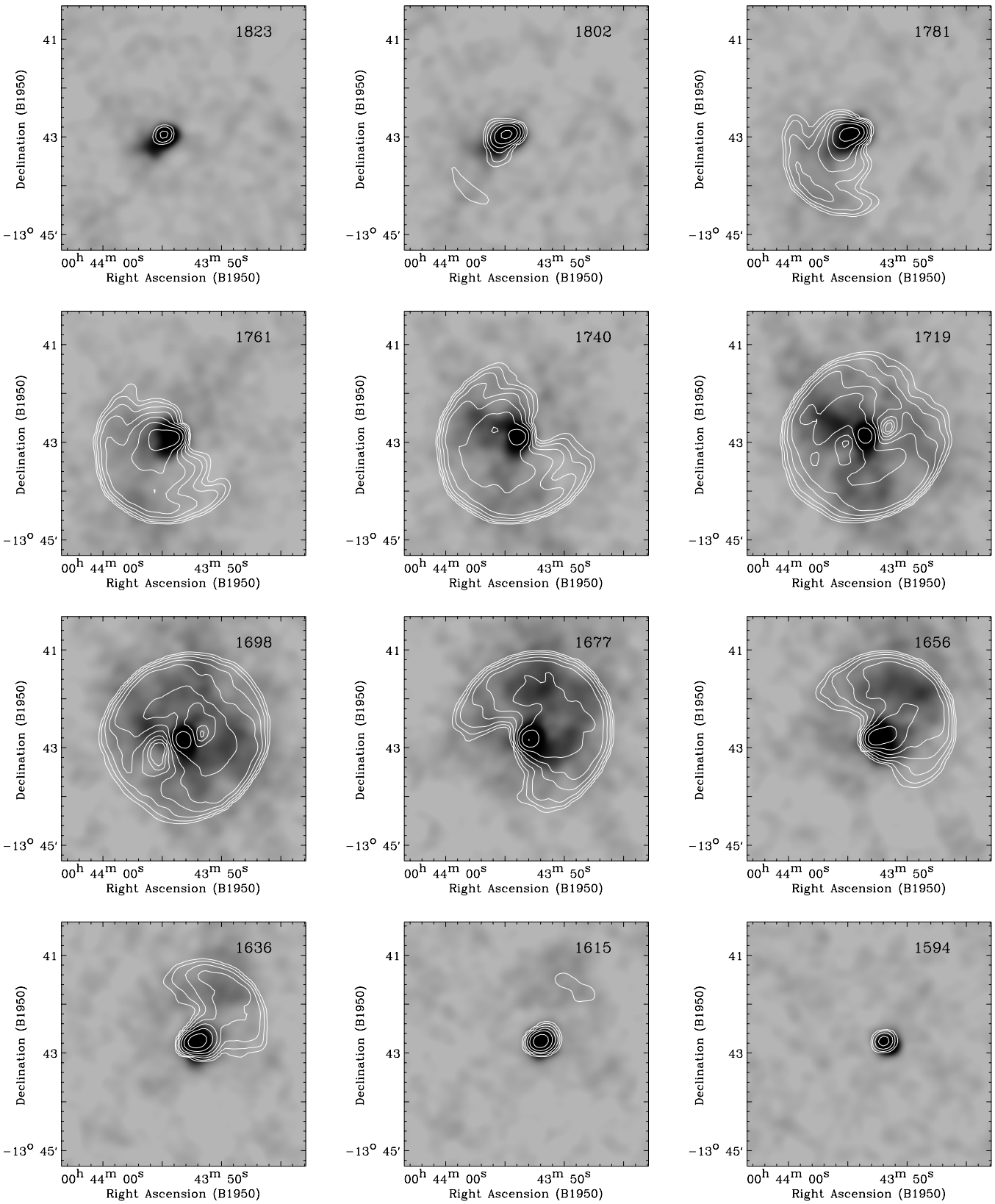

Figure 11. Model channel maps of the H I emission of Arp 230 (contours) superposed on grayscale representations of the data.

two key additional questions that remain: (1) What fraction of the gas remains in a cold (high angular momentum) disk-like component following a shell-producing encounter? and finally (2) How might the fate of this gas relate to future star formation history—will these galaxies build up significant new disks or evolve into spheroids? While the two objects discussed in this paper are in a unique transformative stage, we emphasize that the answers to these questions may have consequences for disk formation, destruction, and regrowth in galaxies at low and high redshift.

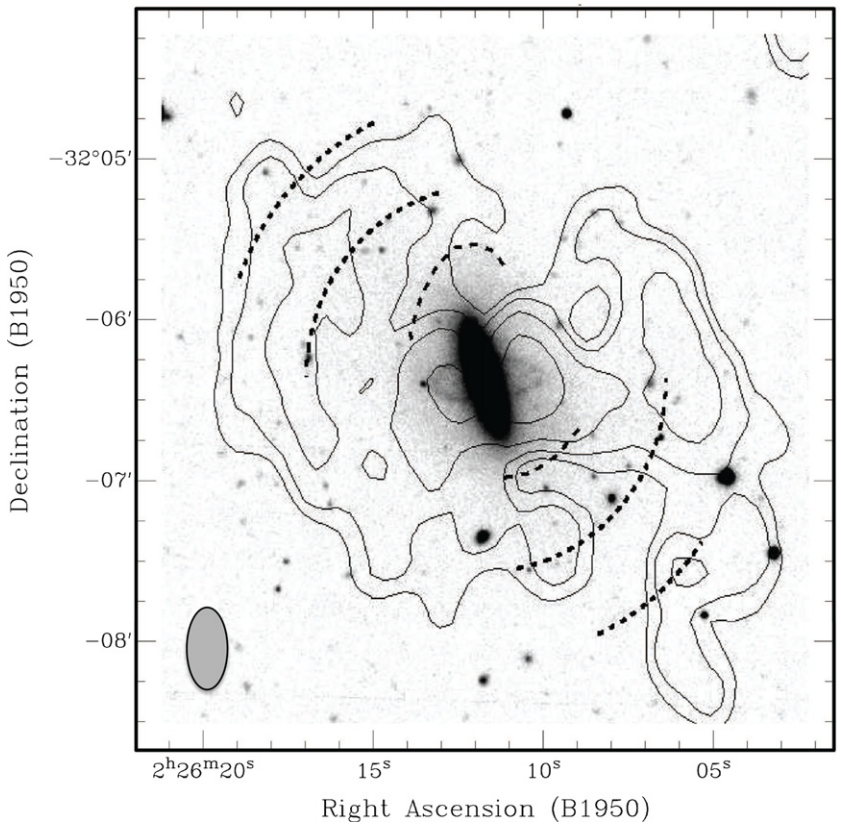

Figure 12. H I distribution of MCG −5-7-1 superposed on the *V* image. Contours are 0.5, 1, 2, 4 $\times 10^{20}$ cm^{-2}.

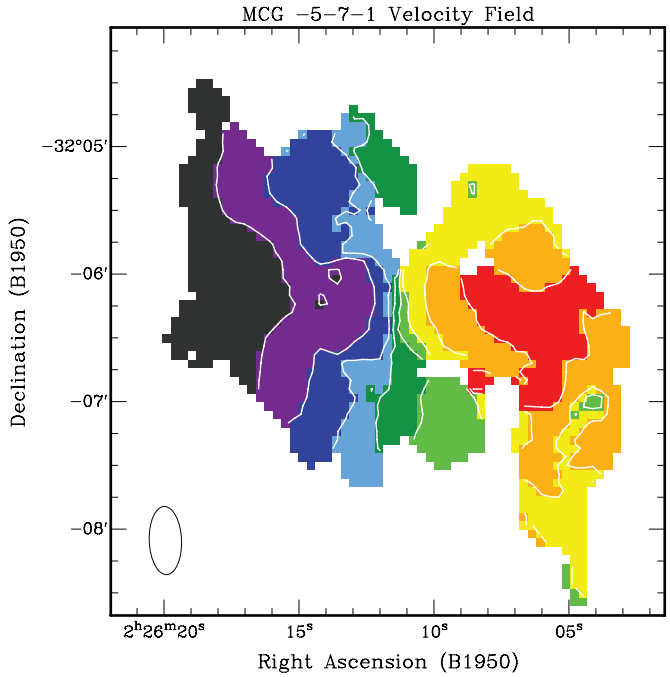

Figure 13. Velocity field of MCG −5-7-1. Contours are 4450, 4490, 4530, 4570, 4610, 4650, 4690, and 4730 km s^{-1} (from red to black).

5.1. M/L Ratio and the Shape of the Potential

In principle one can use the H I kinematics to probe the mass distribution in shell galaxies provided that H I is mostly settled in undisturbed orbits. A natural complication with shell ellipticals is that the dynamical youth that makes them good candidates for possessing extended H I also makes them poor candidates for dynamical studies, since we expect the gas in these systems to be largely unsettled. Yet, the rather surprising regularity of the velocity fields for both Arp 230 and MCG −5-7-1, as well as the regularity observed in other shell systems (Cen A, NGC 2865) suggests that our intuition concerning the various dynamical timescales at work is incorrect and that we can use the H I kinematics to probe the underlying potential. Below we discuss briefly how our observations might constrain the mass-to-light ratio and the shape of the underlying mass distribution.

We determined how the mass-to-light ratio varies with radius for both galaxies. At a distance of 24.4 Mpc, the maximum projected linear extent of the detected H I in Arp 230 is 13.6 kpc (114″). We take 85^{+40}_{-10} km s^{-1} as the maximum rotational velocity from rotation curve fits, taking into account the possibility that we have underestimated the velocity due to beam smearing in the inner regions and shallow inclination effects in the outer regions. The derived rotational period is then 1000^{+140}_{-300} h^{-1} Myr. Furthermore, assuming circular orbits around a central mass, the total enclosed mass at this radius is $1.6^{+1.9}_{-.3} \times 10^{10} M_{\odot}$ giving us an M/L_B of $2.4^{+2.8}_{-.6}$ h.

At a distance of 65.6 Mpc, the maximum projected linear extent of the detected H I in MGC-5-7-1 is 40 kpc (126″). We take 180^{+20}_{-20} km s^{-1} as the maximum rotational velocity from rotation curve fits. The derived rotational period is then 1.4 ± 0.1 Gyr. Furthermore, assuming Keplerian orbits around a central mass, the total enclosed mass at this radius is $3.0 \pm .5 \times 10^{11}\ M_{\odot}$ giving us an M/L_B of 30 ± 7. We examined the mass-to-light ratio as a function of radius using $L_B(r)$ derived from data in Whitmore (this time correcting for inclination effects).

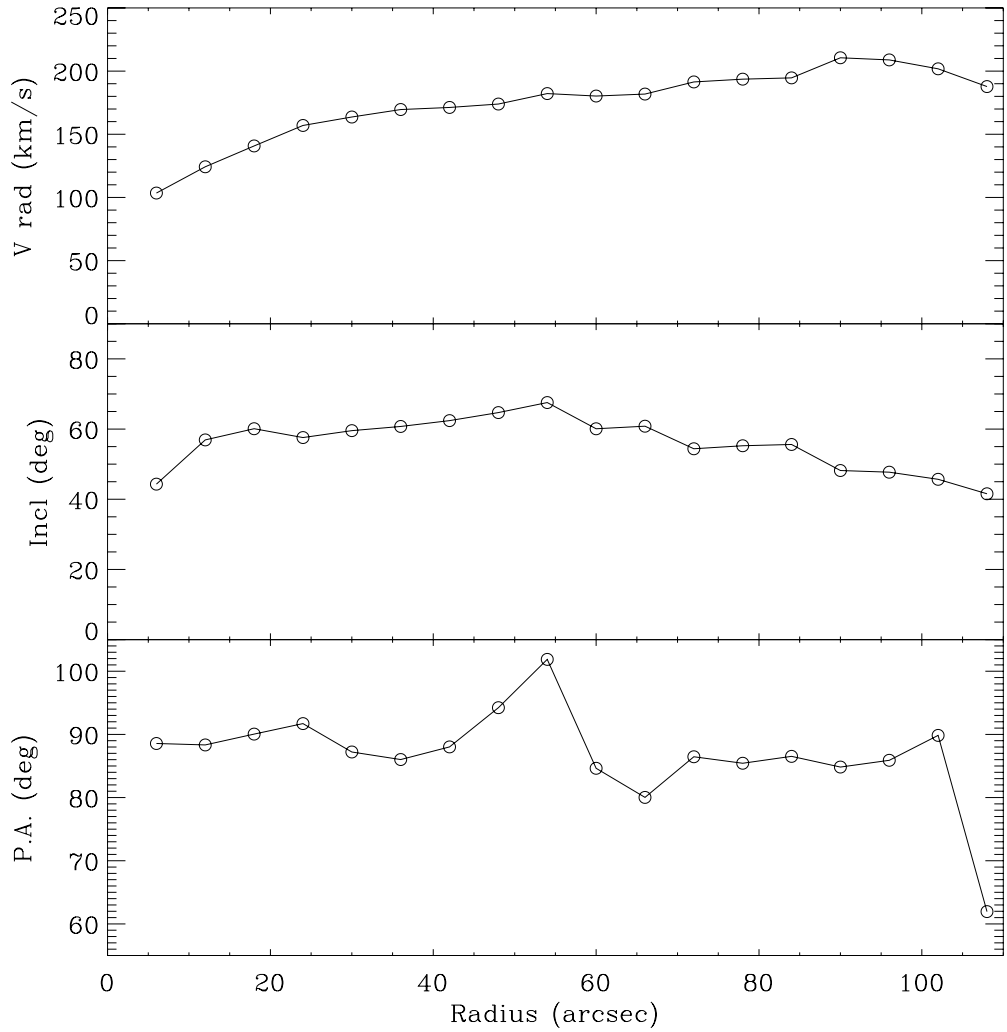

Figure 14. Rotation curve fit for MCG −5-7-1. The panels show (from top to bottom) rotation velocity, inclination, and position angle of the line of nodes as a function of radius.

We find an increase in the mass-to-light ratio with radius of more than a factor of four.

More unique to our study is that we have exploited the gas in different planes to try to characterize the shape of the potential of each galaxy. An important effect is the differential precession which occurs when material follows orbits inclined with respect to a non-spherical potential. If the precession timescale is sufficiently slow compared to the orbital timescale, material that is initially confined to an inclined plane will develop a coherent warp. Stable warps can be produced in tumbling triaxial potentials (e.g., van Albada et al. 1982), or quasi-stable warps can develop in axisymmetric or triaxial potentials (Steiman-Cameron 1984; Steiman-Cameron & Durisen 1982) as seen in the double-ringed systems NGC 2685 and Arp 660 (Mahon 1992).

Sparke (1996) has modeled the orbital precession in Centaurus A (NGC 5128) and has shown that she can explain all of the observed features in the central dust lane (H I, van Gorkom et al. 1990; Hα, Nicholson et al. 1992; CO, Quillen et al. 1992) as well as the extended H I (Schiminovich et al. 1994) using a precessing near-polar disk in an approximately oblate potential (with varying ellipticity). These results predict that the material began precessing ∼0.75 Gyr ago. Are similar processes at work in Arp 230 and MCG −5-7-1? We show below that unstable warps are consistent with some aspects the observed H I, and possibly provide some insight into the shape of the potential around these systems. It is worth keeping in mind that infall of material even in small amounts may also drive a warp (Binney 1992).

Arp 230 displays a nearly edge-on H I disk near the center of the dust lane with a symmetric clockwise bend with radius. Color maps of Arp 230 indicate strong reddening along a highly inclined region near the nucleus (McGaugh & Bothun 1990; Prieur 1988). It is difficult to determine from our data the true inclination of the gas in the very inner regions ($<10''$). Our high-resolution velocity data are consistent with a decrease in inclination in the nucleus. A careful study of the colors, Hα, and dust-lane morphology in the *Hubble Space Telescope* image may enable a better determination of the inner morphology.

We can use our rotation curve fits to compare the inner and outer H I in Arp 230. If we use our measured values at $20''$ and $80''$, we find that the inner and outer gas has angular momentum vectors separated by 49°–68° (or 112°–131°); the H I components are substantially inclined with respect to one another. The galaxy itself is very likely seen nearly face-on, with the outer ring less inclined with respect to the plane of the galaxy than the inner ring. The position–velocity plots show the inner and outer material as two distinct components. Nevertheless, if the H I started in a single plane with the inner material settling toward the polar orbits and the outer material bending toward the

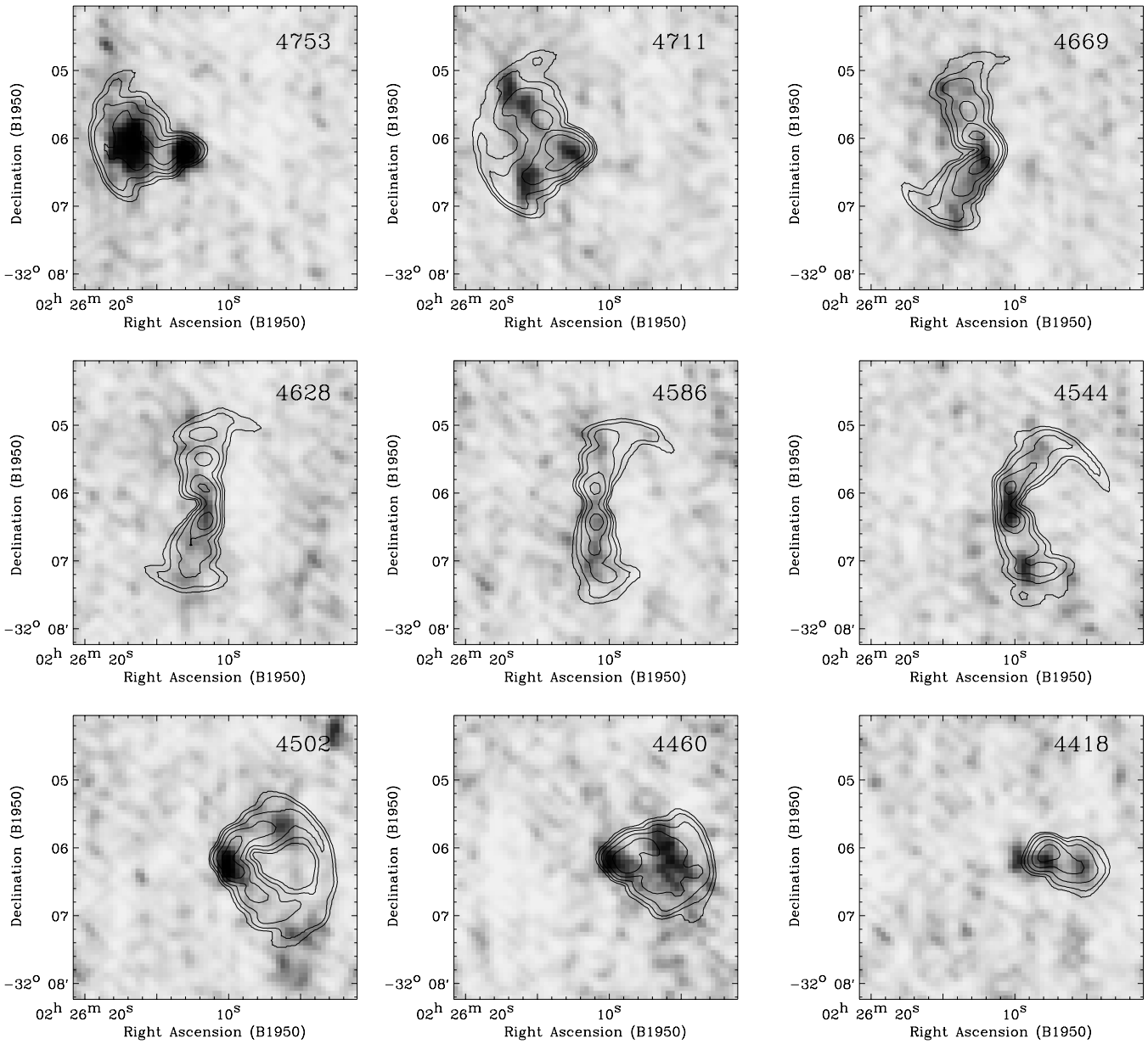

Figure 15. Model channel maps of the H I emission of MCG −5-7-1 (contours) superposed on grayscale representations of the data.

plane of short axis rotation—then it is not unlikely that a break developed at an intermediate radius within the warp (Sparke 1995).

Assuming an unstable configuration, we may consider the ratio between the orbital period and the precession period to obtain a rough estimate for the flattening of an axisymmetric potential. Considering a mean precession angle (30° or 60°) at a radius of ∼40″ gives us a ratio of precession period to orbital period of (24 or 12) suggesting a flattening between 5% and 10% (see Binney & Tremaine 1987). Self-gravity, and other stabilizing torques may allow the potential to flatten further.

Now we consider the orbital geometry of the MCG −5-7-1 system. The polar ring has an inclination of 68°. From the morphology of the dust obscuration, it appears that the ring is inclined so that its northernmost point is obscured by the galaxy (normal vector up and out of the page). Furthermore, the dust morphology suggests that the S0 galaxy is oriented so that its NW side is obscured by the ring (normal vector to the left and out of the page, inclination 106°). This is further supported by the asymmetric Hα distribution. We find the polar ring to be 84° from the plane of the S0, although as noted in van Gorkom et al. (1987), if the S0 were more edge-on this value would decrease to 74°.

Given this geometry we determine from our rotation curve fit, which shows a decrease in inclination with radius, that the rings never exceed 10° from polar. Thus, for MCG −5-7-1, the angular momentum vector of the H I appears to lie close to the plane of the S0, with movement in that plane consistent with a (somewhat) oblate axisymmetric potential with orbits in a plane precessing about the z-axis. Interestingly, this would be true for nearly face-on orbits at the position angle of the shells, for which concentric arcs might seem to imply a nearly face-on (<30°) viewing angle (though the shell axis itself is inclined by only 30° with respect to the S0).

The orbital period for the outer gas in MCG −5-7-1 is 5–6 times longer than that for the inner gas. The angular momentum vector of the outer gas is tilted by no more than 30° with respect to the inner material yielding a ratio of mean

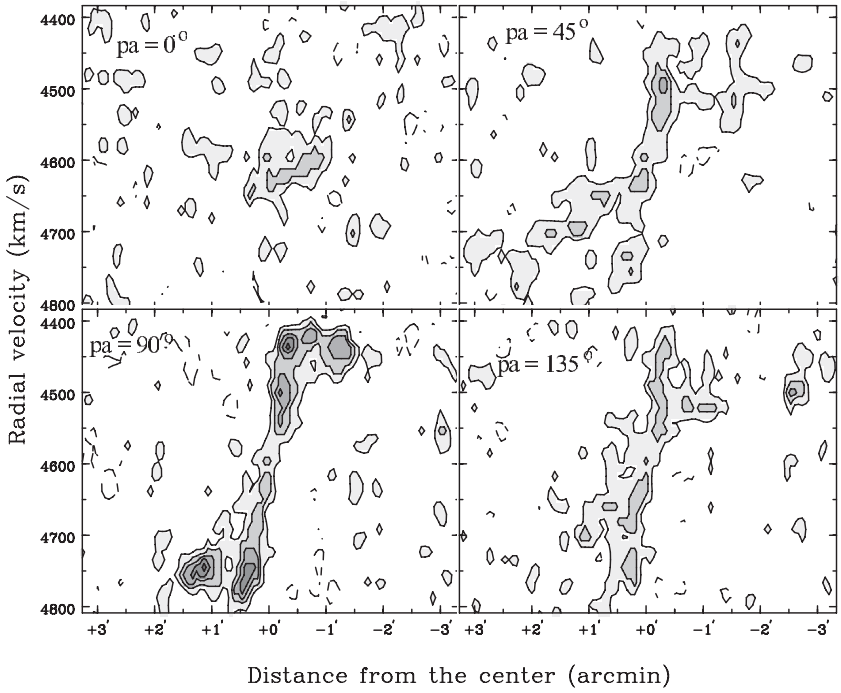

Figure 16. Position–velocity maps of the H I emission in MCG −5-7-1 at position angles of (from top left to bottom right) 0°, 45°, 90°, and 135°. Contours are −0.6, 0.6, 1.2, 1.8, 2.4, 3 mJy beam^{-1}. Major axis position angle is ∼90°.

precession period to mean orbital period of more than 60. This provides further evidence that the potential is not significantly flattened, similar to the findings of Whitmore et al. (1987). It is quite possible that the potential becomes more oblate at intermediate (and larger) radii, as suggested for Cen A by Sparke (1996). It is important to note, however, that self-gravity of the ring, or rotating, non-axisymmetric potentials may help to stabilize the orbits against differential precession, even in a highly flattened potential (e.g., Katz & Rix 1992).

5.2. Gas Evolution in Shell Galaxies and Merger Remnants

The only theoretical studies directly relating to the gas morphology in shell galaxies are the hybrid *N*-body/hydrodynamical simulations (TREESPH; Hernquist & Katz 1989) of gas motions in shell galaxy collisions (Hernquist & Weil 1992; Weil & Hernquist 1993). These studies simulate shell-producing encounters between 10:1 mass ratio progenitors with 10% of the secondary mass in gas. The principal result of these simulations is that most of the gas rapidly segregates from the stars in the secondary and sinks to the center of the primary to form a dense, central gas disk. A number of more elaborate TREESPH studies involving major and minor mergers (Mihos & Hernquist 1994, 1996; Barnes & Hernquist 1996, 1998) confirm similar processes for mergers with varying mass ratios, extending the parameter space explored by Weil & Hernquist (1993).

Although much gas sinks to the center of the merged system, some fraction of the gas will remain in the outer parts of the remnant and retain some memory of the recent encounter (Barnes & Hernquist 1996). Our observations of Arp 230 and MCG −5-7-1, as well as previous findings for NGC 2865, Cen A (Schiminovich et al. 1994, 1995) and NGC 3656 (Sancisi & Balcells 1996; Balcells et al. 2001) clearly show a substantial amount ($>10^8\ M_\odot$) of H I at large radii. In Section 5.3 we will compare our results to subsequent simulations by Barnes (2002), which specifically address the evolution of the gas that fails to reach the nuclei of merger remnants. In this section we address the broader question of the fate of gas in any shell-producing process.

5.2.1. Simple Shell Models

The shell model developed by Quinn (1984) produces shells as the result of "phase wrapping" in a primary potential: stars in shells are turning around in their orbits ($v_{\rm rad} = 0$). This model has the advantage that it reproduces the observed effect that in many ellipticals the shells appear to be aligned with the projected major axis of the underlying galaxy (Prieur 1990).

What will the gas do in such a collision? Consider the simplest phase-wrapping model, with a gas-rich secondary with low specific angular momentum. After the first pass through the primary potential, stars are redistributed radially according to their energy in the potential and then begin their phase-wrapping oscillations. Once phase wrapping begins, every point in space within the phase wrapping (except the outermost unwrapped material) will have stars and gas with crossing orbits. The collisionless stars will survive, but most of the gas will eventually lose energy in collisions and sink to the center of the potential on timescales related to the gas density and filling factor. If a small amount of angular momentum is added to this model (i.e., due to a non-radial encounter), then as some of the gas sinks to the center, the angular momentum must be transported to the gas that remains at larger radii. This angular momentum reduces the amount of orbit crossing and gas collisions, especially for material that has experienced few radial oscillations: gas may mimic a collisionless fluid, like the stars, for a longer time.

It is quite possible that we are observing phase wrapping at work in Arp 230. We see gas at large radii that is associated with the southern plume (or first shell) as we might expect for material that has experienced only two crossings. At smaller radii, however, we do not see gas connected with the radial shells. We do find that a large fraction of the gas has collected at

the center of the galaxy and that the outer gas has substantially more angular momentum than the inner material, as we would expect after collisions have redistributed the angular momentum in this system. For "phase-wrapped" shells stars are at their orbital turning points, so we would expect their velocities to be systemic. Interestingly enough, the H I velocity field shows the gas along the shell axis to have nearly systemic velocities.

The shells in Arp 230 with their beautiful aligned, interleaved morphology could thus very well have been formed in a "head-on" collision with a smaller secondary, very similar to the ones modeled by Quinn (1984).

What if the shells are not the result of phase wraps, but rather are produced by the edge-brightening of loops (or spatially wrapped material; Hernquist & Quinn 1988, 1989; Quillen 1993) orbiting at a large inclination with respect to the line of sight? The H I observations do not appear to support this, since we would expect to see the kinematic major axis aligned with the major axis of the loops, and we would also expect to see more gas associated with the loops at all radii.

Such a scenario might be more applicable to MCG −5-7-1 where we see a slightly better alignment between the kinematic major axis of the gas and the axis of the shells (especially the outermost shells). The major axis of the outer gas distribution falls close to the shell axis. We also observe H I near several shells with the gas morphology mimicking the curvature and angular extent of the shells. That the gas is not directly coincident with the shells, but is displaced to the outside similar to what is observed in NGC 5128 and NGC 2865, could reflect the patchy nature of the gas distribution. Long timescale gas-dynamical processes (weak collisions, winds) might also explain the displacement.

In MCG −5-7-1, the gas associated with the shells falls close to the kinematic major axis. Regardless of whether shells are phase wraps or edge-brightened folds and loops, the sharp faint edge that we observe is most probably in or near the plane of the sky; the line between the center of the shell and the center of the galaxy would then be the geometric line of nodes of the orbits of the stars in the shell. For circular orbits, we expect the kinematic major axis to be aligned with the line of nodes; non-circular orbits will show deviations (Binney 1992; Teuben 1991; Franx et al. 1994). We might be able to use shells as fiducial marks (just as rings are used for constraining motions) to determine the nature of the gas/star orbits and possibly to extract more information about the underlying potential or gas-dynamical properties. Thus far, a number of the shells where associated gas has been detected have shown an approximate alignment, though in nearly all cases deviations are seen (a notable exception is the SW gas of Cen A). This indicates that we are observing non-circular motions or more complex geometries, with folds and wraps far above or below the plane of the sky.

5.2.2. Internal Processes (Secular Evolution)

The models considered above all have in common that the gas we observe in these galaxies has been stolen from neighboring companions, has been accreted in a minor merger, or has resulted from the wholesale formation of the galaxy in a major merger. Other possibilities are internal scenarios for shell formation (Thomson 1992; Struck & Smith 1999). So far we have not considered such internal scenarios.

Our observations revealed total H I masses of $1.2 \times 10^9\ M_\odot$ in Arp 230 and $3.7 \times 10^9\ M_\odot$ in MCG −5-7-1. Though these masses are not exceptional for early-type galaxies with detected H I, they are considerably higher than usually found in early types. The high H I masses, the association (or counterassociation) of the H I with the optical peculiarities of these systems, and the fact that the H I does not appear to be rotating in the principal plane of either galaxy, suggests that the gas is not of internal origin.

In addition it is worth noting that the shell axis in MCG −5-7-1 twists toward the major axis of the S0 at small radii. If successive loops of stellar material are settling toward the plane of the S0 at small radii, as might be suggested by the shell morphology, and if we take the rotation of the shell material to be in the same direction as the gas, then we find that the shell material is counterrotating with respect to the main body (unlike what we observe in Cen A and NGC 2865). This counterrotation also rules out internal scenarios for shell formation. So from here on we will only consider accretion/merger scenarios and consider the environment of Arp 230 and MCG −5-7-1.

5.2.3. Major Merger Scenario

The environments of Arp 230 (see Figure 17) and MGC –5-7-1 (see Figure 18) have notable differences. Arp 230 is isolated with no nearby dwarfs or companions of known redshift (NED). The nearest neighbors, a group of four galaxies, are 0.6 Mpc away. Arp 230 is part of a void (Void 11; El-Ad & Piran 1997). The absence of significant H I emission in the VLA cubes confirms that Arp 230 resides in a predominantly gas-poor region of space. The 3σ limit for H I detections is $7 \times 10^7 M_\odot$ assuming a size of $1'$ or 7 kpc and a velocity width of 60 km s^{-1}. MCG −5-7-1 is in a slightly denser environment. Its closest neighbor is at a projected distance of only 100 kpc (NED), while there are another five, randomly distributed galaxies within a projected distance of 0.6 Mpc. None of these were detected in the VLA cubes to a 3σ limit of $3 \times 10^8\ M_\odot$. It is not very likely that Arp 230 accreted stars and gas from other galaxies during the past 1–2 Gyr. For MCG −5-7-1 this is less obvious. It could have accreted material from its closest companion, though the timescales are still fairly long.

A more probable scenario then is that gas was brought into these systems from either a major or minor merger (Schweizer 1983). The H I content of both systems is high enough, $>10^9 M_\odot$, that it appears unlikely that a typical dwarf irregular (Matthews et al. 1995, 1996; Gallagher et al. 1995) carried the gas unless more than one accretion event took place. More likely, the gas (and shells) resulted from an encounter with another disk galaxy with mass ratio between 1:10 and 1:1 (Hernquist & Spergel 1992; Mihos & Hernquist 1994, 1996). The faint, red, possibly counterrotating, shells of MCG −5-7-1 suggest a minor merger. The bright, blue shells and blue body of Arp 230 might very well have resulted from a nearly equal mass merger of small late-type spirals. In either of the two systems, but Arp 230 in particular, the extended gas and aligned shell systems could very well have formed out of the infalling material from tidal debris following a major merger (Hibbard & Mihos 1995).

Since we have not modeled these two systems, we cannot estimate ages based on the observed inclinations of the successive rings of material. However, the settled kinematics suggest that all of the H I has orbited the galaxy at least once, possibly more (Rix & Katz 1991). Therefore, we can use this to set a lower limit to the age of the systems of about half a billion years. These ages are quite consistent with ages determined from the observed shell morphology.

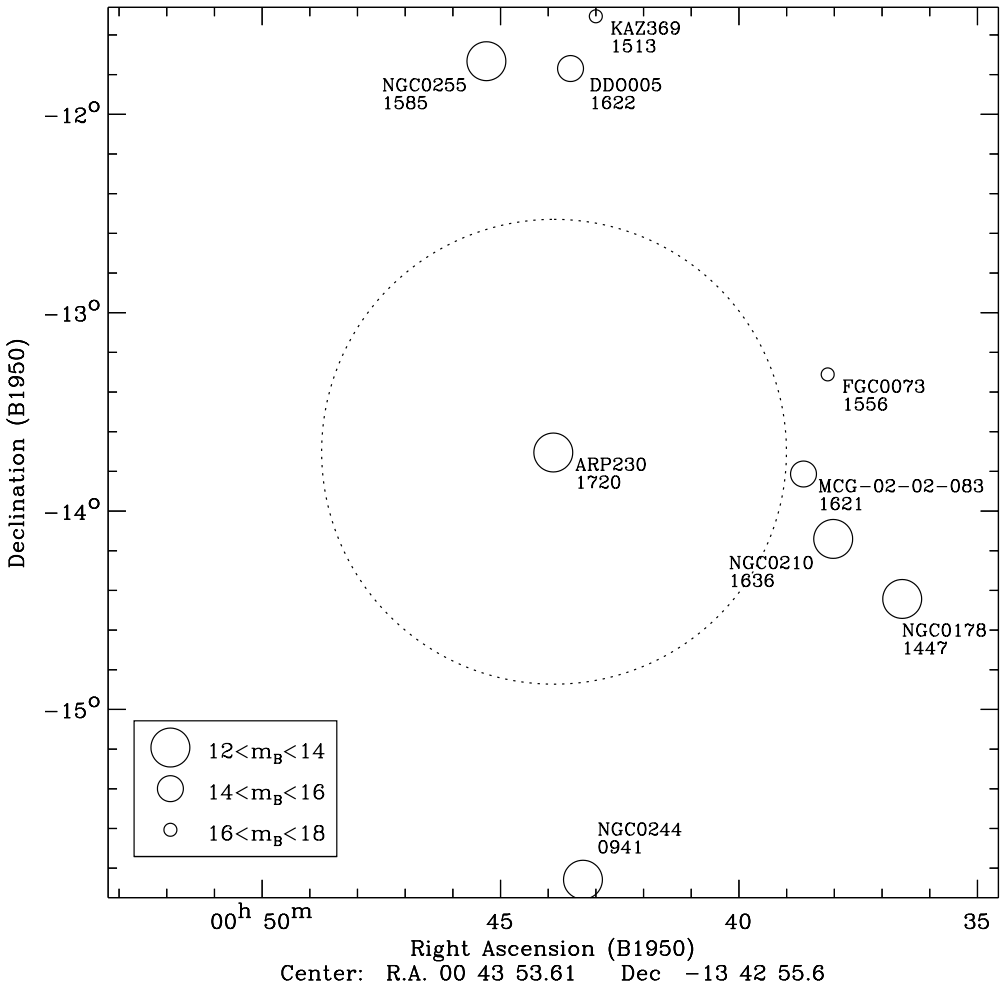

Figure 17. Nearby environment for Arp 230. Plotted are all galaxies in NED within a radius of 2.2 deg (1.0 Mpc) and with radial velocities between 700 and 2700 km s^{-1}. The dotted circle corresponds to a 500 kpc radius at the distance of Arp 230.

In this picture the formation of these systems is ongoing, with gradual differential precession, gas-dynamical settling, and continuing star formation. With its extensive dust lane and large supply of gas, Arp 230 could quite possibly become a radio galaxy similar to Cen A, should it possess a central engine. It is not clear whether either galaxy will ever look like a present-day "normal" elliptical (or S0), since the present gas and dust content exceed by an order of magnitude the cold gas content of typical ellipticals. So to evolve to a "normal" elliptical these objects require efficient star formation, a gas-removal mechanism or a source of energy which ionizes the $\sim 2 \times 10^9 M_\odot$ of gas.

5.3. New Disks or Spheroids?

Given the detection of a significant cold gas reservoir around these galaxies it is natural to consider its implications for the future star formation histories of these galaxies. First, we determine how these galaxies compare to a representative sample of galaxies in the local universe, by looking at estimates of their stellar mass and star formation rate. We then consider the present-day star formation and gas accretion and then speculate on future paths that these galaxies might follow. Corollary multiwavelength photometry used for this analysis are listed in Table 5 and derived physical properties are provided in Table 6.

Neither Arp 230 nor MCG −5-7-1 is a particularly massive galaxy. Using *K*-band luminosities and color-based mass-to-light ratios from Bell et al. (2003a, 2003b) we derive stellar masses of $8.7 \times 10^9\ M_\odot$ for Arp 230 (host galaxy) and $5.8 \times 10^{10}\ M_\odot$ for MCG −5-7-1. These masses are close to and straddle the "transition mass" between massive bulge-dominated passive galaxies and star-forming disk galaxies detected in the Sloan Digital Sky Survey (SDSS; e.g., Kauffmann et al. 2003). Using

Table 5
Corollary Measurement Data

Property	Unit	Arp 230	MCG −5-7-1	Reference
FUV		16.09	19.65	*GALEX*
NUV		15.55	18.35	*GALEX*
B		13.62 ± 0.18	n/a	RC3
R		13.3	13.2	
J		11.24 ± 0.02	11.59 ± 0.02	2MASS LGC
H		10.60 ± 0.03	10.96 ± 0.03	2MASS LGC
K		10.24 ± 0.04	10.70 ± 0.04	2MASS LGC
IRAS flux (12 μm)	Jy	0.156 ± 0.044	n/a	*IRAS* FSC
IRAS flux (25 μm)	Jy	4.7	n/a	*IRAS* FSC
IRAS flux (60 μm)	Jy	2.2	n/a	*IRAS* FSC
IRAS flux (100 μm)	Jy	4.7	n/a	Cox & Sparke (2004)
Radio (20 cm)	mJy	24.0	n/a	Cox & Sparke (2004)
Radio (20 cm)	mJy	10.7	n/a	Cox & Sparke (2004)
Radio slope		−0.67	n/a	Cox & Sparke (2004)
$E(B-V)$		0.019	0.017	Schlegel Dust Map
AFUV/ANUV		0.152	0.136	Schlegel Dust Map

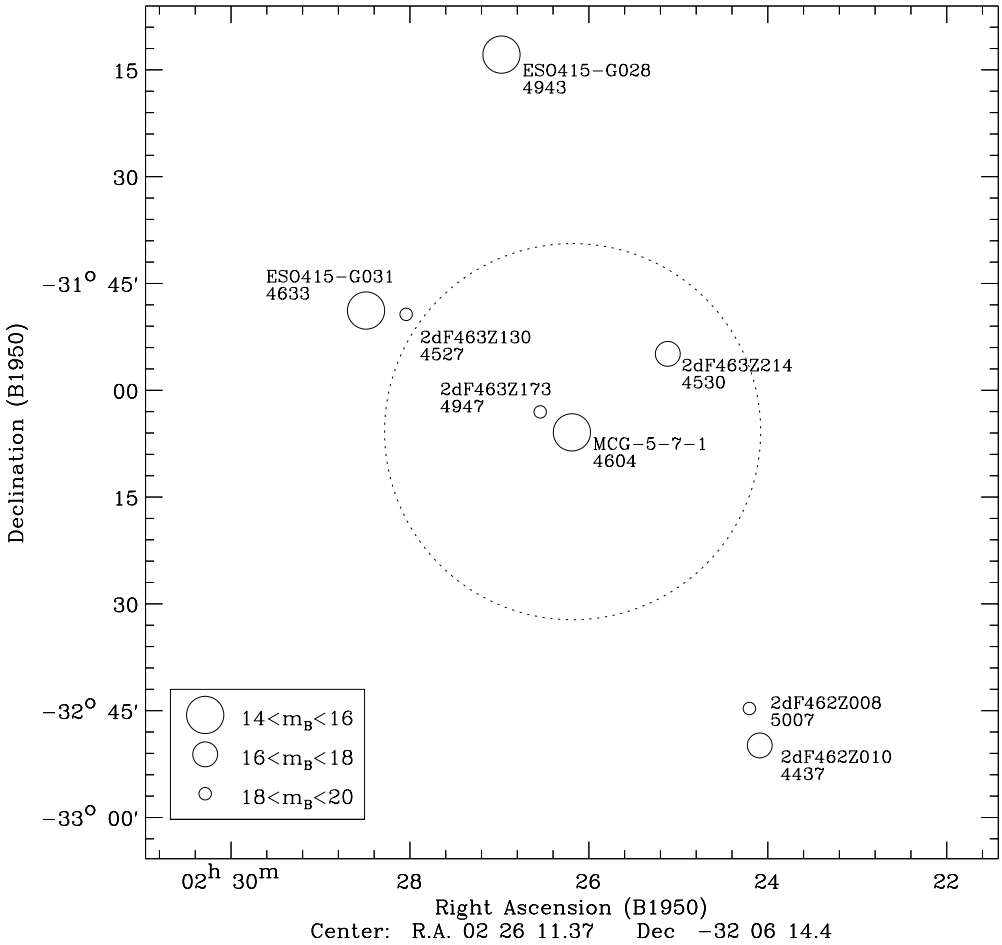

Figure 18. Nearby environment for MCG −5-7-1. Plotted are all galaxies in NED within a radius of 1 deg (1.2 Mpc) and with radial velocities between 3600 and 5600 km s^{-1}. The dotted circle corresponds to a 500 kpc radius at the distance of MCG −5-7-1.

Table 6
Derived Physical Properties

Parameter	Arp 230	MCG −5-7-1
Distance modulus	31.8	34.5
NUV–R	2.25	5.1
$B-R$	0.45	1.44
M_R	−18.6	−20.9
M_K	−18.5	−21.3
L_K ($L_\odot$)	1.0×10^{10}	4.8×10^{10}
$M_\star$ ($M_\odot$)	8.7×10^{9}	5.8×10^{10}
$M_{\rm H\,I}$ ($M_\odot$)	1.2×10^{9}	3.7×10^{9}
$M_{\rm H\,I+H_2}$ ($M_\odot$)	2.8×10^{9}	8.9×10^{9}
$M_{\rm dyn}$ ($M_\odot$)	1.6×10^{10}	2.2×10^{11}
$L_{\rm B}$ ($L_\odot$)	3.9×10^{9}	9.6×10^{9}
$M/L_{\rm B}$	$4.1^{+3.0}_{-0.6}$	24.0 ± 7
$M_{\rm H\,I+H_2}/M_*$	0.32	0.15
$M_{\rm H\,I}/M_{\rm dyn}$	0.075	0.017
$M_{\rm H_2}/M_{\rm H\,I}$	1.33	1.41
SFR ($M_\odot$ yr^{-1})	4	0.5
SFR/$M_\star$ (yr^{-1})	4.6×10^{-10}	8.6×10^{-12}
$M_{\rm H\,I+H_2}$/SFR (yr)	7×10^{8}	1.7×10^{10}

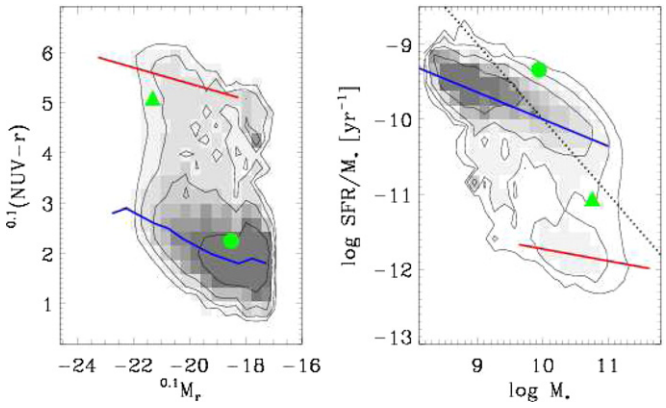

Figure 19. UV–optical colors vs. absolute magnitude and SFR/$M_\star$ vs. $M_\star$ for Arp 230 (green circle) and MCG −5-7-1 (green triangle) vs. distribution for local sample generated using *GALEX* and SDSS (e.g., Schiminovich et al. 2007). Derived values for Arp 230 and MCG −5-7-1 are taken from the table in the text. UV–optical colors have not been corrected for dust attenuation but they have been corrected for Galactic reddening.

(A color version of this figure is available in the online journal.)

the derivations discussed above, the present-day star formation rates of Arp 230 and MCG −5-7-1 are 4 and 0.5 $M_\odot$ yr^{-1}, respectively. Using these values we show in Figure 19 where the two galaxies lie on the UV–optical color–magnitude diagram and the SFR/$M_\star$ versus $M_\star$ relation, using a local sample generated using *Galaxy Evolution Explorer* (*GALEX*) ultraviolet measurements of the SDSS spectroscopic sample (Wyder et al. 2007; Schiminovich et al. 2007). Not surprisingly, we find that Arp 230 has slightly redder NUV–r colors than others of a similar luminosity, which is likely due to the effect of attenuation from dust, and we find that MCG −5-7-1 is slightly bluer than

the galaxies on the "red sequence," likely due to the presence of ongoing and recent star formation, lying in the UV–optical "green valley."

After applying the appropriate dust corrections and stellar mass-to-light ratios we see that in fact Arp 230 appears to be forming stars at a rate higher than even the typical star formation sequence (or blue sequence) galaxy at its stellar mass. Arp 230 is experiencing an enhanced star formation episode, consistent with its unsettled appearance. MCG −5-7-1 is also bluer than the typical red-sequence galaxy (although it is redder than some star-forming galaxies at similar masses), suggesting in this case that it may also be in transition. It is hard to determine whether or not MCG −5-7-1 might be in the process of being quenched as it moves from blue to red, or in the process of forming a new disk as it transitions from the red sequence back to the blue sequence.

The gas masses of each galaxy (H+H_2) are $4 \times 10^9\ M_\odot$ and $1 \times 10^{10}\ M_\odot$ for Arp 230 and MCG −5-7-1, respectively. Thus in both cases, the amount of remaining gas is comparable to their stellar mass, suggesting that given the current gas supply, maximal efficiency in star formation could produce a doubling in stellar mass. If all of this stellar mass were to be generated in a disk, then the resulting bulge to disk ratios would decrease significantly.

For Arp 230 the star formation rate of $4\ M_\odot\ \mathrm{yr}^{-1}$ implies a gas consumption time of 1 Gyr. This is very different for MCG −5-7-1 where upper limits on the far-IR (FIR) luminosity suggest a present-day star formation rate $<1\ M_\odot\ \mathrm{yr}^{-1}$ and therefore a gas consumption timescale in excess of 10 Gyr. Thus the future histories of these galaxies are likely to be quite different, with Arp 230 sustaining a continued burst of star formation at modest intensity while MCG −5-7-1 may harbor low levels of continued star formation fed by a significantly massive outer gas disk.

While gas falling into the nuclei of merging galaxies has been extensively studied, less is known about the fate of the gas that fails to reach the nucleus of the merger remnant. Arp 230 and MCG −5-7-1, though both most likely merger remnants, have large amounts of H I that may not ever fall into the center. Much of the H I is located at large radii from the center and it is rotating rapidly. Barnes (2002) presents simulations to study the fate of the gas in the outer parts of merger remnants. He finds for a range of mass ratios and orbital parameters that up to half of the gas in the progenitors settles into embedded disks. The most massive disks result from encounters in which both galaxies are inclined to the orbital plane. The disks are often warped and show complex kinematics. The disks grow typically from the inside out; infall from tidal tails may continue disk formation over long periods of time. Arp 230 appears to be a good example of this, with it inner, warped disk of gas, MCG −5-7-1 differs in that it has formed an inner, even more massive gaseous ring, but no disk.

We can use the present H I observations to estimate the gas surface densities in the inner and outer disks and compare these with the typical threshold densities for star formation (Skillman 1987; Kennicutt 1989; Bigiel et al. 2010), which are close to $10^{21}\ \mathrm{cm}^{-2}$ or $8\ M_\odot\ \mathrm{pc}^{-2}$. If we take the size of the central disk or ring in Arp 230 to be 7.3 kpc with an inner radius of 1.8 kpc then the average H I surface density is $\sim 12\ M_\odot\ \mathrm{pc}^{-2}$, above the typical star formation threshold. In the outer parts the H I surface density is much lower: $\sim 1.2\ M_\odot\ \mathrm{pc}^{-2}$, well below the threshold, supporting the lack of star formation in the outer H I disk. The situation in MCG −5-7-1 is similar, except that the H I surface densities in the inner ring/disk are just around the threshold, $\sim 8\ M_\odot\ \mathrm{pc}^{-2}$, correcting for resolution taking the dimensions of the optical polar ring. In the outer parts the H I surface densities drop below $\sim 2\ M_\odot\ \mathrm{pc}^{-2}$.

The disk of Arp 230 is more typical of the minor axis dust lanes in ellipticals than the prototypical polar ring around S0s. The estimated H I surface densities in the inner regions appear consistent with the significant ongoing star formation in Arp 230, very much like the central dust lane in Centaurus A, and the very modest star formation in the thin ring around MCG −5-7-1. CO measurements (Bettoni et al. 2001; adjusted to our distances) indicate that in the central disks H_2/H I ratios well above 1 for both Arp 230 and MCG −5-7-1, but that does not alter the relative picture sketched above.

Might these systems be distinguished by the rate of steady state gas infall? We can make estimates of the gas infall rate in the two systems by requiring at least one orbit for the outermost material. For MCG −5-7-1 this provides us with a lower limit to the age ∼1.5 Gyr. Since the H I mass in the ring is 30% of the total H I mass, we find that at least $12.2 \times 10^8 M_\odot$ of H I has settled into the ring, this being a lower limit since we know that star formation and conversion to other phases has very likely occurred in the ring. The infall rate is then $\lesssim 0.9\ M_\odot\ \mathrm{yr}^{-1}$ of H I with infall velocities $\lesssim 25\ \mathrm{km\ s}^{-1}$. Similarly, for Arp 230, we can estimate a gas infall rate. Once again we require at least one orbital period for the outer material. The inner ring contains ∼75% of the total H I mass of $8.2 \times 10^8\ M_\odot$, suggesting for an orbital period of 1.0^{-1} Gyr, a mass infall rate of $\sim 0.85\ M_\odot\ \mathrm{yr}^{-1}$ of H I with infall velocities $\lesssim 15\ \mathrm{km\ s}^{-1}$. Arp 230 and MCG −5-7-1 are very similar in their inferred steady state infall rate.

Richter et al. (1994) found that confirmed polar rings were similar to regular early-type galaxies in terms of their FIR luminosity, while the more disturbed or merging systems in the polar-ring catalog are much more IR luminous. This suggests that the warped disks with enhanced star formation rates might be the result of rapid gas inflow following episodic encounters, mergers, or accretion in the lifetime of these systems. These processes efficiently drive gas to the nuclei of the galaxies. Simulations have shown (Weil & Hernquist 1993; Barnes & Hernquist 1996, 1998; Mihos & Hernquist 1994, 1996) that encounters involving gas can produce central rings rather than disks if a collision is sufficiently non-radial. This would indeed be consistent with our interpretation of the origin of the shell/gas morphology in Arp 230 and MCG −5-7-1.

5.4. Conclusions

We have presented detailed imaging of the H I in two shell galaxies: Arp 230 and MCG −5-7-1. The main surprise is the very regular kinematics suggesting the presence of a fairly settled disk of H I in addition to a dense inner H I disk or ring. The outer H I disk shows little association with the optical shells in Arp 230, while there is some correspondence with the optical shells in MCG −5-7-1.

Thus far Arp 230 is unique in that it is so far the only shell galaxy where the H I characteristics appear to favor a "phase-wrapped" case resulting from a nearly radial collision: the radial shells are found in regions where the velocities are around the systemic velocities and which the higher angular momentum H I appear to avoid.

MCG −5-7-1 is more likely to be the result of a "spatially wrapped" case resulting from a 1:10 mass ratio merger. Internal formation scenarios are ruled out by the observations.

The H I disks probably are fairly well settled, judging from what the surprisingly regular kinematics indicate and we used the H I kinematics to set limits to the mass distribution of the underlying galaxies. The potentials appear only slightly flattened (5%–10%) and the galaxies have M/L_B ratios of $2.4^{+2.0}_{-0.6}$ (Arp 230) and M/L_B of 30 ± 7 (MCG −5-7-1). The ratios change as a function of radius because of the presence of a dark halo in both systems.

The star formation rates in the inner disk of Arp 230 and the polar ring of MCG −5-7-1 appear consistent with the estimated H I surface densities. Arp 230 has a compacter, higher density central disk, with a higher star formation rate than MCG −5-7-1. Arp 230 is very similar to Centaurus A in this respect. Furthermore, we (re-)emphasize in this paper that shell galaxies such as MCG −5-7-1, along with previously studied galaxies NGC 5128 (Cen A) and NGC 2865, are unique in that they provide evidence of recent accretion with gas and collisionless stars showing clear association, though the displacement suggests the presence of significant gas-dynamical interaction.

We thank John Hibbard and Francois Schweizer for discussions and nagging us to publish our results on these interesting galaxies. We thank the anonymous referee for suggestions that improved the manuscript. The VLA is operated by the National Radio Astronomy Observatory. The National Radio Astronomy Observatory is a facility of the National Science Foundation operated under cooperative agreement by Associated Universities, Inc.

This research has made use of the NASA/IPAC Extragalactic Database (NED) which is operated by the Jet Propulsion Laboratory, California Institute of Technology, under contract with the National Aeronautics and Space Administration.

REFERENCES

Arp, H. C. 1966, ApJS, 14, 1
Arp, H. C., & Madore, B. F. 1986, Catalogue of Southern Peculiar Galaxies and Associations (Cambridge: Cambridge Univ. Press)
Baars, J. W. M., Genzel, R., Pauliny-Toth, I. I. K., & Witzel, A. 1977, A&A, 61, 99
Balcells, M., van Gorkom, J. H., & Sancisi, R. 2001, AJ, 122, 1758
Barnes, J. E. 2002, MNRAS, 333, 481
Barnes, J. E., & Hernquist, L. 1996, ApJ, 471, 115
Barnes, J. E., & Hernquist, L. 1998, ApJ, 495, 187
Begeman, K. 1987, PhD dissertation, Univ. Groningen
Begeman, K. 1989, A&A, 223, 47
Bell, E. F., McIntosh, D. H., Katz, N., & Weinberg, M. D. 2003a, ApJS, 149, 289
Bell, E. F., McIntosh, D. H., Katz, N., & Weinberg, M. D. 2003b, ApJL, 585, 117
Bettoni, D., Galletta, G., Garciá-Burillo, S., & Rodríguez-Franco, A. 2001, A&A, 374, 421
Bigiel, F., Leroy, A., Walter, F., et al. 2010, AJ, 140, 1194
Binney, J. 1992, ARA&A, 30, 51
Binney, J., & Tremaine, S. 1987, Galactic Dynamics (Princeton, NJ: Princeton Univ. Press)
Briggs, D. S. 1995, BAAS, 187, 112.02
Brook, C. B., Governato, F., Quinn, T., et al. 2008, ApJ, 689, 678
Charmandaris, V., Combes, F., & van der Hulst, J. M. 2000, A&A, 356, L1
Clark, B. 1980, A&A, 89, 377
Combes, F., & Charmandaris, V. 1999, in ASP Conf. Ser. 192, Galaxy Dynamics, ed. D. R. Merritt, M. Valura, & J. A. Sellwood (San Francisco, CA: ASP), 489
Cornwell, T. J., Uson, J. M., & Haddad, N. 1992, A&A, 258, 583
Cox, A. L., & Sparke, L. S. 2004, AJ, 128, 2013
El-Ad, H., & Piran, T. 1997, ApJ, 491, 421
Fort, B. P., Prieur, J.-L., Carter, D., Meatheringham, S. J., & Vigroux, L. 1986, ApJ, 306, 110
Franx, M., van Gorkom, J. H., & de Zeeuw, P. T. 1994, ApJ, 436, 642
Gallagher, J. S., III, Littleton, J. E., & Matthews, L. D. 1995, AJ, 109, 2003
Galletta, G., Sage, L. J., & Sparke, L. S. 1997, MNRAS, 284, 773
Hernández-Toledo, H. M., Vázquez-Mata, J. A., Martínez-Vázquez, L. A., et al. 2008, AJ, 136, 2115
Hernquist, L., & Katz, N. 1989, ApJS, 70, 419
Hernquist, L., & Quinn, P. J. 1988, ApJ, 331, 628
Hernquist, L., & Quinn, P. J. 1989, ApJ, 342, 1
Hernquist, L., & Spergel, D. N. 1992, ApJ, 399, 117
Hernquist, L., & Weil, M. L. 1992, Natur, 358, 734
Hibbard, J. E., & Mihos, J. C. 1995, AJ, 110, 140
Hopkins, P. F., Somerville, R. S., Cox, T. J., et al. 2009, MNRAS, 397, 802
Iodice, E., Arnaboldi, M., Sparke, L. S., Gallagher, J. S., & Freeman, K. C. 2002, A&A, 391, 103
Katz, N., & Rix, H.-W. 1992, ApJ, 395, 113
Kauffmann, G., Heckman, T. M., White, S. D. M., et al. 2003, MNRAS, 341, 33
Kennicutt, R. C., Jr. 1989, ApJ, 344, 685
Mahon, M. E. 1992, PhD thesis, Univ. Florida
Malin, D. F., & Carter, D. 1983, ApJ, 274, 534
Matthews, L. D., & Gallagher, J. S., III. 1996, AJ, 111, 1098
Matthews, L. D., Gallagher, J. S., III, & Littleton, J. E. 1995, AJ, 110, 581
Martínez-Delgado, D., Peñarrubia, J., Gabany, R. J., et al. 2008, ApJ, 689, 184
McGaugh, S. S., & Bothun, G. D. 1990, AJ, 100, 1073
Mihos, J. C., & Hernquist, L. 1994, ApJ, 425, 13
Mihos, J. C., & Hernquist, L. 1996, ApJ, 464, 641
Nicholson, R. A., Bland-hawthorn, J., & Taylor, K. 1992, ApJ, 387, 503
Prieur, J.-L. 1988, ApJ, 326, 596
Prieur, J.-L. 1990, in Dynamics and Interactions of Galaxies, ed. R. Wielen (Berlin: Springer), 72
Quillen, A. C. 1993, PhD thesis, California Institute of Technology
Quillen, A. C., de Zeeuw, P. T., Phinney, E. S., & Phillips, T. G. 1992, ApJ, 391, 121
Quinn, P. J. 1984, ApJ, 279, 596
Richter, O.-G., Sackett, P. D., & Sparke, L. 1994, AJ, 107, 99
Rix, H.-W., & Katz, N. 1991, in Warped Disks and Inclined Rings Around Galaxies, ed. S. Casertano, P. D. Sackett, & F. H. Briggs (Cambridge: Cambridge Univ. Press), 112
Rogstad, D. H., Lockart, I. A., & Wright, M. C. H. 1974, ApJ, 193, 309
Sancisi, R., & Balcells, M. 1996, AJ, 111, 1053
Schiminovich, D., van Gorkom, J. H., van der Hulst, J. M., & Kasow, S. 1994, ApJL, 423, 101
Schiminovich, D., van Gorkom, J. H., van der Hulst, J. M., & Malin, D. F. 1995, ApJL, 444, 77
Schiminovich, D., Wyder, T. K., Martin, D. C., et al. 2007, ApJS, 173, 315
Schweizer, F. 1983, AJ, 88, 909
Schweizer, F., & Seitzer, P. 1992, AJ, 104, 1039
Schweizer, F., & Seitzer, P. 1988, ApJ, 328, 88
Skillman, E. D. 1987, in Star formation in Galaxies, ed. Carol J. Lonsdale Persson (NASA Conf. N87-24266; Washington, D. C.: NASA), 263
Sparke, L. 1995, ApJ, 439, 42
Sparke, L. 1996, ApJ, 473, 810
Steiman-Cameron, T. Y. 1984, PhD thesis, Univ. Indiana
Steiman-Cameron, T. Y., & Durisen, R. H. 1982, ApJL, 263, 51
Strauss, M. A., Huchra, J. P., Davis, M., et al. 1992, ApJS, 83, 29
Struck, C., & Smith, D. C. 1999, ApJ, 527, 673
Tal, T., & van Dokkum, P. G. 2011, ApJ, 731, 89
Teuben, P. J. 1991, in Warped Disks and Inclined Rings Around Galaxies, ed. S. Casertano, P. D. Sackett, & F. H. Briggs (Cambridge: Cambridge Univ. Press), 40
Thomson, R. C. 1992, MNRAS, 257, 689
Thronson, H. A., Jr., Bally, J., & Hacking, P. 1989, AJ, 97, 363
van Albada, T. S., Kotanyi, C. G., & Schwarzschild, M. 1982, MNRAS, 198, 303
van Dokkum, P. G., Franx, M., Förster Schreiber, N. M., et al. 2004, ApJ, 611, 703
van Gorkom, J. H., Schechter, P. L., & Kristian, J. 1987, ApJ, 314, 457
van Gorkom, J. H., van der Hulst, J. M., Haschick, A. D., & Tubbs, A. D. 1990, AJ, 99, 1781
Weil, M. L., & Hernquist, L. 1993, ApJ, 405, 142
Whitmore, B. C., Lucas, R. A., McElroy, D. B., et al. 1990, AJ, 100, 1489
Whitmore, B. C., McElroy, D. B., & Schweizer, F. 1987, ApJ, 314, 439
Wilkinson, A., Browne, I. W. A., & Wolstencroft, R. D. 1987, MNRAS, 228, 933
Wyder, T. K., Martin, D. C., Schiminovich, D., et al. 2007, ApJS, 173, 293